

# A Consistent Reaction Scheme for the Selective Catalytic Reduction of Nitrogen Oxides with Ammonia

Ton V. W. Janssens,<sup>†</sup> Hanne Falsig,<sup>†</sup> Lars F. Lundegaard,<sup>†</sup> Peter N. R. Vennestrøm,<sup>†</sup> Søren B. Rasmussen,<sup>†</sup> Poul Georg Moses,<sup>†</sup> Filippo Giordano,<sup>‡</sup> Elisa Borfecchia,<sup>‡</sup> Kirill A. Lomachenko,<sup>‡,¶</sup> Carlo Lamberti,<sup>‡,¶</sup> Silvia Bordiga,<sup>\*,†</sup> Anita Godiksen,<sup>§</sup> Susanne Mossin,<sup>\*,§</sup> and Pablo Beato<sup>\*,†</sup>

<sup>†</sup>Haldor Topsøe A/S, Nymøllevvej 55, 2800 Kgs. Lyngby, Denmark

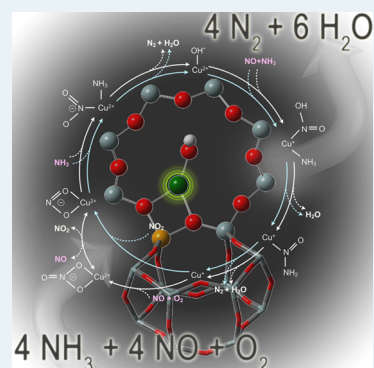
<sup>‡</sup>Department of Chemistry, INSTM Reference Center, University of Turin, Via Giuria 7, 10125 Torino, Italy

<sup>¶</sup>Southern Federal University, Zorge Street 5, 344090 Rostov-on-Don, Russia

<sup>§</sup>Centre for Catalysis and Sustainable Chemistry, Department of Chemistry, Technical University of Denmark, Kemitorvet 207, 2800 Kgs. Lyngby, Denmark

**ABSTRACT:** For the first time, the standard and fast selective catalytic reduction (SCR) of NO by NH<sub>3</sub> are described in a complete catalytic cycle that is able to produce the correct stoichiometry while allowing adsorption and desorption of stable molecules only. The standard SCR reaction is a coupling of the activation of NO by O<sub>2</sub> with the fast SCR reaction, enabled by the release of NO<sub>2</sub>. According to the scheme, the SCR reaction can be divided into an oxidation of the catalyst by NO + O<sub>2</sub> and a reduction by NO + NH<sub>3</sub>; these steps together constitute a complete catalytic cycle. Furthermore, both NO and NH<sub>3</sub> are required in the reduction, and finally, oxidation by NO + O<sub>2</sub> or NO<sub>2</sub> leads to the same state of the catalyst. These points are shown experimentally for a Cu-CHA catalyst by combining in situ X-ray absorption spectroscopy (XAS), electron paramagnetic resonance (EPR), and Fourier transform infrared spectroscopy (FTIR). A consequence of the reaction scheme is that all intermediates in fast SCR are also part of the standard SCR cycle. The activation energy calculated by density functional theory (DFT) indicates that the oxidation of an NO molecule by O<sub>2</sub> to a bidentate nitrate ligand is rate-determining for standard SCR. Finally, the role of a nitrate/nitrite equilibrium and the possible influence of Cu dimers and Brønsted sites are discussed, and an explanation is offered as to how a catalyst can be effective for SCR while being a poor catalyst for NO oxidation to NO<sub>2</sub>.

**KEYWORDS:** SCR, fast SCR, rate-determining step, mechanism, Cu-CHA, NO oxidation, EPR, EXAFS, FTIR, XANES, DFT



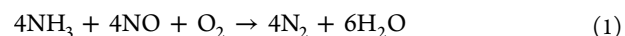
## 1. INTRODUCTION

The selective catalytic reduction (SCR) of NO to N<sub>2</sub> by ammonia (NH<sub>3</sub>-SCR) plays an important role in the abatement of NO<sub>x</sub> emissions in the exhausts of diesel engines and power plants. With environmental legislation becoming more stringent in many places in the world, this reaction is going to play an important role in the development of technologies to meet the emission requirements for exhaust gases. The commercially available catalysts for exhaust gas cleaning by NH<sub>3</sub>-SCR are based on vanadium oxide supported on titanium oxide, Fe-exchanged zeolites, or Cu-exchanged zeolites. The traditional zeolites applied in SCR are ZSM-5, and zeolite β. More recently, Cu-exchanged chabazites (CHA), in particular SSZ-13 and SAPO-34, have become more important because these materials are more stable under high temperature conditions. Other known Cu- or Fe-exchanged zeolites with SCR activity are SSZ-39,<sup>1</sup> ferrierite, and mordenite.<sup>2,3</sup>

The composition and temperature of the exhaust gas from which the NO is to be removed depends on the source. In an automotive diesel engine, a typical exhaust gas contains up to a few hundred parts per million of NO<sub>x</sub>, 5–10% water vapor, 5–

10% O<sub>2</sub>, hydrocarbons, CO, and CO<sub>2</sub>. Ammonia is usually introduced by decomposition of urea to a concentration level of typically 1.0–1.2 times the NO concentration; the slight excess of ammonia ensures an efficient removal of the NO. In a typical exhaust aftertreatment system, the hydrocarbons and CO are removed upstream from the SCR catalyst, and hence, the SCR catalyst is exposed to a mixture of NO<sub>x</sub>, O<sub>2</sub>, H<sub>2</sub>O, and NH<sub>3</sub> in an inert gas (N<sub>2</sub> and CO<sub>2</sub>). The temperature at the SCR catalyst varies, and it is generally required that the SCR catalyst performs well in the temperature range 200–500 °C. This gas composition and temperature range define the general operation conditions for an SCR catalyst system.

The key reaction in the NH<sub>3</sub>-SCR is the formation of nitrogen from NO and NH<sub>3</sub> according to the equation

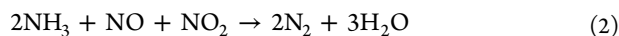


Received: October 29, 2014

Revised: February 22, 2015

Published: March 19, 2015

This reaction is often referred to as “standard SCR”. In the presence of NO<sub>2</sub>, nitrogen can also be formed according to



Because this reaction is faster than the standard SCR reaction,<sup>4</sup> it is often referred to as “fast SCR”. In addition to these two reactions, a number of side reactions can occur in the mixture of NO<sub>x</sub>, O<sub>2</sub>, H<sub>2</sub>O, and NH<sub>3</sub>, such as formation of N<sub>2</sub>O, or ammonia oxidation to NO<sub>x</sub>. These side reactions do not directly contribute to the transformation of NO and NH<sub>3</sub> to N<sub>2</sub>, but have an impact on the performance of the SCR catalyst because they influence the selectivity for N<sub>2</sub>.

Because of the number of possible reactions in this system, the chemistry involved in the NH<sub>3</sub>-SCR reaction is rather complex. Consequently, the reaction mechanism for the NH<sub>3</sub>-SCR is still under discussion. In this article, first the key aspects of the SCR reaction mechanism are reviewed, and some shortcomings with the proposed reaction schemes are identified. Then we present a new reaction scheme that resolves these shortcomings in the present schemes and corroborate the reaction scheme by means of density functional theory (DFT) calculations, X-ray absorption spectroscopy (XAS), electron paramagnetic resonance (EPR), and Fourier transform infrared spectroscopy (FTIR) by example of a Cu-CHA catalyst. Finally, the consequences of the proposed mechanism are discussed, leading to new insights in the role of the different reactants and intermediates, and in the chemistry behind the SCR reaction.

## 2. MECHANISTIC ASPECTS OF THE SCR REACTION

As mentioned in the introduction, the best known catalysts for SCR are supported vanadium oxide on titanium oxide and Cu- and Fe- exchanged zeolites. All the catalysts based on vanadium oxide and ion-exchanged zeolites have an activity for redox reactions and acidic properties. For a V-based catalyst, a mechanism combining an acid cycle with a redox cycle was proposed. In the acid cycle, the ammonia is adsorbed and reacts with NO to N<sub>2</sub> and H<sub>2</sub>O, while reducing V<sup>5+</sup> to V<sup>4+</sup>; the redox cycle restitutes the V<sup>5+</sup> state of the catalyst through oxidation by oxygen and water.<sup>5</sup> This scheme involves transfer of an H atom from adsorbed NH<sub>3</sub> to a neighboring V<sup>5+</sup>=O site. According to such a reaction scheme, at least two neighboring V atoms are involved in the SCR reaction.<sup>5,6</sup> The SCR reaction can also take place on a single V atom,<sup>7</sup> but the SCR reaction becomes significantly faster with the presence of polymeric V species.<sup>8</sup>

In the Cu- and Fe-exchanged zeolites, the oxidation properties are related to the ability of the exchanged ions to change oxidation state.<sup>9,10</sup> In general, such catalysts also have Brønsted acidity because either the standard procedures for Cu or Fe exchange do not result in a complete exchange or new protonic sites are formed as a result of a reduction of the metal ions.<sup>11</sup> It is argued that the exchanged Cu or Fe ions facilitate the SCR reaction<sup>9,12–14</sup> by oxidizing the NO to NO<sub>2</sub>, whereas the SCR reaction takes place elsewhere in the zeolite,<sup>15,16</sup> which could be on the ammonia adsorbed on the Brønsted sites. If the Brønsted sites are located close to the Cu (or Fe) ions in the zeolite, it is conceivable that an NO<sub>2</sub> molecule on a Cu ion can interact directly with an NH<sub>3</sub> molecule on a neighboring Brønsted site, which would make a reaction possible without the need for desorption of NO<sub>2</sub>.<sup>17</sup> Such an interaction between an oxidation site and an acid site resembles that for the vanadium oxide catalyst, as mentioned above.

A consequence of the redox/acid cycle scheme is that the SCR activity of an ion-exchanged zeolite becomes quite sensitive to the amount and distribution of the Al atoms in the framework of the zeolites.<sup>18–21</sup> However, the role of the Brønsted sites in an ion-exchanged zeolite is not well understood at present. For Cu-MFI and Cu-CHA zeolites, it was found that the SCR activity at 200 °C is not dependent on the number of Brønsted sites in these materials. This indicates that either the Brønsted sites do not play a role in the SCR reaction or these sites are always saturated with NH<sub>4</sub><sup>+</sup> ions under reaction conditions.<sup>12,22</sup> Likewise, Brønsted sites in Fe-MFI catalysts are generally not required for high activity, but they could influence the distribution of the Fe ions or act as a promoter for the active Fe ions.<sup>23,24</sup> All these results indicate that the SCR reaction takes place on the metal ions in Cu or Fe zeolites, with a limited influence of the Brønsted sites, at most.

The distribution of the Al-framework atoms in a zeolite also affects the ability to form Cu or Fe dimers. After ion exchange, the Cu atoms are coordinated to the oxygen atoms in Si–O–Al bridges, probably as a Cu<sup>2+</sup>–OH<sup>−</sup> unit,<sup>13,25–29</sup> which has a total charge of +1 to balance the negative charge on the Si–O–Al site. Two neighboring Cu<sup>2+</sup>–OH<sup>−</sup> or Cu<sup>+</sup> units can combine to form a Cu–O–Cu structure,<sup>30–39</sup> which is bound to two different Al atoms in the framework. On the basis of the observation that the activity per Cu atom increases with the Cu-loading,<sup>39,40</sup> it has been suggested that the formation of such Cu dimers enhances the SCR activity of Cu-SSZ-13.

In Cu zeolites, the local environment of the Cu ions may be important for the SCR activity. Recently, it has been shown that the Cu ions in a Cu-CHA zeolite are located in both the 6- and 8-rings of the chabazite framework structure.<sup>28,29,34,41</sup> Upon adsorption of NH<sub>3</sub>, NO, or H<sub>2</sub>O on the Cu atoms in the 6-rings, the Cu atoms are lifted out from their original position into the larger cavities in the zeolite,<sup>42–44</sup> and therefore, it seems that the SCR reaction actually takes place in the large cavities in Cu-CHA; however, only the Cu ions located in or close to the 6-rings seem to contribute to the SCR activity in Cu-CHA.<sup>12,45–48</sup>

Independent of the nature and structure of the catalyst and the local environment of the active sites, the SCR reaction can be divided into a reduction part and an oxidation part, quite similar to the well-known Mars–Van Krevelen scheme for oxidation reactions. The reduction part corresponds to the steps in which the ammonia reacts with the NO to nitrogen, and the catalytic site is reduced. In the mechanism for SCR over supported vanadium oxide mentioned above, the acid cycle would represent the reduction part of the reaction. For Cu zeolites, it has been proposed that the reduction takes place by adsorption of both NO and NH<sub>3</sub> on Cu<sup>2+</sup>, leading to the formation of an ammonium nitrite or nitrate-like species, which decomposes to N<sub>2</sub> and H<sub>2</sub>O, while the Cu<sup>2+</sup> is reduced to Cu<sup>+</sup>.<sup>40,49–51</sup> The presence of Cu<sup>+</sup> has been unambiguously identified by XAS under SCR conditions and infrared spectroscopy, even though the amounts may vary, depending on the zeolite type<sup>10,12,47,52,53</sup> and the steady-state conditions of the SCR reaction. This direct observation of Cu<sup>+</sup> confirms the idea that the SCR activity originates from the ability of the exchanged Cu to change the oxidation state. In addition to NH<sub>3</sub>, NO also plays a role in the reduction part of the SCR reaction.<sup>10,40,51</sup> The formation of a Cu<sup>+</sup>–NO<sup>+</sup> species<sup>25,54</sup> by adsorption of NO onto Cu<sup>2+</sup> at room temperature suggests that the Cu is actually reduced by NO. On Fe-exchanged zeolites, the reduction follows essentially the same scheme as on Cu-

exchanged zeolites, with a reduction of  $\text{Fe}^{3+}$  to  $\text{Fe}^{2+}$  under the influence of  $\text{NH}_3$  and  $\text{NO}$ .<sup>10,15</sup> However, Fe-zeolites show a more pronounced inhibition by  $\text{NH}_3$  for the SCR reaction, as compared with Cu-zeolites.<sup>10,55</sup>

Whereas the reduction part of the SCR reaction seems quite well understood, the oxidation part is less clear. The oxidation part includes both the reoxidation of the catalytic site and the activation of NO. The reoxidation of the active site closes the catalytic cycle. This part of the reaction is often associated with the  $\text{O}_2$  that is needed for the SCR reaction, according to eq 1.<sup>5,9,10,40</sup> The detailed steps describing this part of the reaction, however, are not known. An unsolved problem is that a single Cu or Fe ion increases the oxidation state by only 1, for example, from  $\text{Cu}^+$  to  $\text{Cu}^{2+}$ , and hence, delivers only one electron, whereas an oxygen molecule requires four electrons to be reduced to water. As a consequence, if the oxidation reaction would take place with  $\text{O}_2$  only, a single oxygen molecule must interact with four Cu or Fe ions. Therefore, it is likely that the oxidation of the catalytic site is accompanied by another oxidation reaction at that site, such as the oxidation of NO. This means that the activation of NO and the restoration of the catalytic site always occur together.

It is often argued that an activation of NO to (adsorbed)  $\text{NO}_2$  is necessary for the SCR reaction.<sup>15</sup> On the basis of the fact that the SCR reaction becomes much faster in the presence of  $\text{NO}_2$ , this step has also been proposed as the rate-determining step for the standard SCR reaction.<sup>56–59</sup> The adsorbed  $\text{NO}_2$  is the first step in the formation of reactive nitrate and nitrite species,<sup>15,40</sup> which could occur by disproportionation of two  $\text{NO}_2$  molecules to  $\text{NO}_3^-$  and  $\text{NO}^+$  or, alternatively, by a reaction between NO and  $\text{NO}_2$  via an  $\text{N}_2\text{O}_3$  intermediate.<sup>40</sup> In the presence of  $\text{NH}_3$  and  $\text{H}_2\text{O}$ ,  $\text{N}_2\text{O}_3$  and  $\text{NO}^+$  react further to ammonium nitrite  $\text{NH}_4\text{NO}_2$ , which readily decomposes to  $\text{N}_2$  and water.<sup>15,40</sup> The  $\text{NO}_3^-$  species are transformed to ammonium nitrate, which upon decomposition may produce  $\text{N}_2\text{O}$ .<sup>40</sup>

Nitrates have also been considered as important intermediates for the fast SCR reaction over vanadium oxide-based catalysts. In particular it has been noticed that nitrates react with NO to give  $\text{NO}_2$ .<sup>60,61</sup> This reaction is not confined to vanadium oxide-based systems because exposure of nitrates in Cu- or Fe-exchanged zeolites to NO also results in a transient release of  $\text{NO}_2$ .<sup>55,62–64</sup> The opposite reaction also occurs: a direct exposure of an SCR catalyst to  $\text{NO}_2$  results in the formation of some NO.<sup>55,59,62,65</sup> This indicates that nitrates can be converted to nitrites and vice versa, depending on the gas atmosphere.

The conclusion that the oxidation of NO by  $\text{O}_2$  to  $\text{NO}_2$  is the rate-determining step in the SCR reaction is challenged by Ruggeri et al.<sup>66</sup> They compare the rate of NO oxidation over a Cu zeolite with the rate of the SCR reaction and show that the NO oxidation is much slower in the entire temperature range 200–550 °C and that the effect of water is quite different for the NO oxidation compared with the SCR reaction. It is argued that if the  $\text{NO}_2$  formation were a part of the SCR reaction, then the rates of the NO oxidation and SCR reactions should be similar, as well as the effect of water on them. Following this argument, the formation of  $\text{NO}_2$  cannot be part of the SCR reaction. A point against this reasoning is that  $\text{NO}_2$  can be formed but does not desorb from the Cu sites under the given conditions.<sup>59,61,64,67</sup> In that case, the SCR reaction would involve a reaction of adsorbed  $\text{NO}_2$  with ammonia adsorbed on Cu, not on the Brønsted sites. Temperature-programmed

desorption of  $\text{NO}_2$  on Cu-CHA, however, shows that the onset of  $\text{NO}_2$  desorption is around 300 °C and that the desorption is complete around 450 °C.<sup>59,61</sup> This would imply that, at least above 450 °C, the rate of  $\text{NO}_2$  formation should approach that of the SCR reaction if the desorption of  $\text{NO}_2$  were rate-limiting. Ruggeri et al. suggest that the rate-determining steps for SCR and  $\text{NO}_2(\text{g})$  formation are different: for NO oxidation, it is the release of  $\text{NO}_2$  from a surface nitrite; for SCR, it is the reaction of surface nitrites with  $\text{NH}_3$ .<sup>66</sup> At this time, it is not known why Cu-exchanged zeolites are effective SCR catalysts and at the same time poor catalysts for the oxidation of NO to  $\text{NO}_2$ .

In conclusion, there have been several proposals for the mechanism for the SCR reaction. The consensus is that  $\text{N}_2$  is formed by a reaction between ammonia and a (N, O) species, which is accompanied by a reduction of the catalytic site. It is also clear that the oxidation of NO plays a role in the reoxidation of the catalytic site. However, we note that most of the proposed reaction schemes are not able to produce the stoichiometry of the SCR reaction as given in eq 1 in a closed catalytic cycle. Often, single oxygen atoms, fractional molecules ( $(1/2)\text{O}_2$ ) or isolated ions, such as  $\text{H}^+$ ,  $\text{OH}^-$ , and  $\text{O}^{2-}$ , are invoked. Such species are not readily available and also imply other changes to the catalyst: the use of a single  $\text{H}^+$  ion leaves an isolated negative charge on the catalyst, or the second oxygen atom in  $(1/2)\text{O}_2$  must be accommodated in the catalyst. These changes have to be restored, as well, to close the catalytic cycle. In the following, we construct a reaction scheme for the SCR reaction on a Cu-exchanged zeolite, which is consistent with the stoichiometry of the SCR reaction as given in eq 1, and involves only adsorption and desorption of stable molecules. The proposed reaction scheme is supported by spectroscopy and DFT calculations. Some implications of the reaction scheme are discussed, leading to new insights in the SCR reaction and a deeper understanding of the role of NO,  $\text{NH}_3$ ,  $\text{NO}_2$ , and the adsorbed nitrate (and nitrite) species, which are often observed in situ and operando spectroscopic studies of the SCR reactions.

### 3. A CONSISTENT REACTION SCHEME FOR SCR

The variety of proposed reaction schemes for the SCR reaction in the literature is a consequence of the fact that several different reactions can occur simultaneously in a gas mixture of  $\text{NO}/\text{NH}_3/\text{O}_2/\text{H}_2\text{O}$  in the presence of an oxidation catalyst with acidic properties. In most cases, the proposed reaction schemes are based on in situ spectroscopic observations of certain species, and it is then attempted to give these particular species a place in the reaction scheme. The problem with this approach is that it is hard to determine if a given species that is observed actually plays a role in the SCR reaction, is part of a side reaction, or is just a spectator species.<sup>68</sup> Obviously, this complicates the process of finding a consistent reaction scheme for the SCR reaction.

To overcome that problem, we have taken a different approach. Instead of starting with a number of possible reaction intermediates, we have focused on the SCR reaction as given in eq 1 and attempted to outline how this reaction could proceed on a Cu-exchanged zeolite, given that the reaction gas mixture contains  $\text{O}_2$ , NO,  $\text{NO}_2$ ,  $\text{NH}_3$ ,  $\text{N}_2$ , and  $\text{H}_2\text{O}$ . Furthermore, we imposed the following requirements:

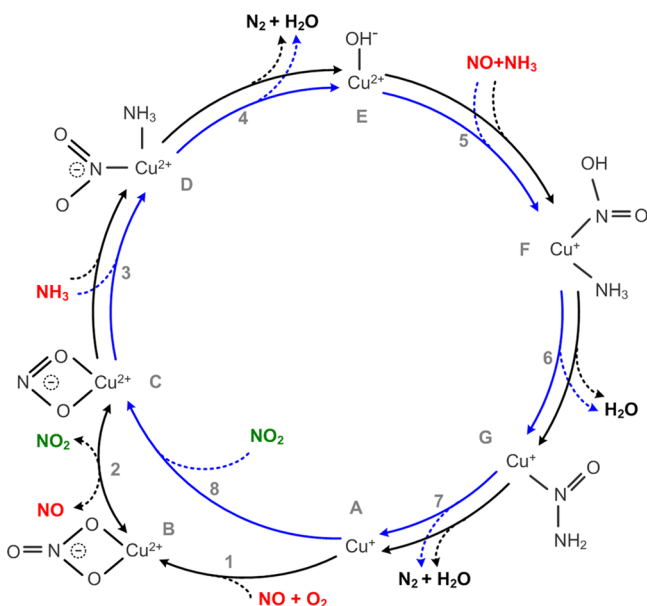
1. In each reaction step, the mass balance is maintained, and the complete catalytic cycle is consistent with the total stoichiometry of the SCR reaction, eq 1;

- adsorption from and desorption to the gas phase can take place only with stable molecules—O<sub>2</sub>, NO, NO<sub>2</sub>, NH<sub>3</sub>, N<sub>2</sub>, and H<sub>2</sub>O—implying that adsorption or desorption of fragments, such as (1/2)O<sub>2</sub>, or isolated ions, for example, OH<sup>-</sup>, H<sup>+</sup>, O<sup>2-</sup>, is not allowed;
- the oxidation state for the active Cu ion changes from 2+ to 1+ in the reduction part, and from 1+ to 2+ in the oxidation part;
- in each step, the charge balance is maintained and the total charge of the Cu complexes in the zeolite is always 1+, allowing for coordination to a single Si–O<sup>-</sup>–Al site in the zeolite.

In this way, we construct a reaction scheme for the SCR reaction only, which means that we do not consider side reactions, such as oxidation of NH<sub>3</sub> by O<sub>2</sub>, or the formation of N<sub>2</sub>O.

Scheme 1 shows a reaction scheme for a Cu-zeolite that fulfills all of the requirements mentioned above. This reaction

### Scheme 1. Proposed Reaction Mechanism for the SCR Reaction in a Cu-zeolite<sup>a</sup>



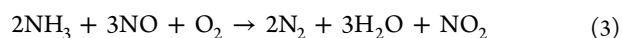
<sup>a</sup>The fast SCR cycle is represented in blue, and the NO activation cycle is represented in black. Reactants are indicated in red, reaction products are indicated in black, and the NO<sub>2</sub> intermediate is indicated in green. In the standard SCR reaction, eq 1, the NO activation cycle, and fast SCR cycle run at equal rates; the stoichiometry of the standard SCR reaction is then found by adding these two cycles. The oxidation states of the Cu ions have been assigned according to the magnetic moment found in DFT:  $M(\text{Cu}^{2+}) > 0.45$  and  $M(\text{Cu}^{+}) < 0.1$ .

scheme can be regarded as the simplest possible reaction path for the SCR reaction.

The key point in this reaction scheme is the formation of an NO<sub>2</sub> molecule in the gas phase by reaction of NO with an adsorbed nitrate species, leaving a nitrite species on the Cu atom (step 2). The NO<sub>2</sub> molecule reacts with a Cu<sup>+</sup> ion elsewhere in the zeolite to an identical nitrite species (step 8). Both nitrites react with ammonia and NO and release water and nitrogen via Cu<sup>2+</sup>–OH<sup>-</sup> species to a Cu<sup>+</sup>; this corresponds to the reduction part of the SCR reaction. The Cu<sup>+</sup> site then reacts either with NO and O<sub>2</sub> or with NO<sub>2</sub> to form the nitrate and nitrite species, closing the catalytic cycle. This corresponds

to the oxidation part of the SCR reaction. Scheme 1 shows that it is conceivable that the entire SCR reaction can take place on a single, isolated Cu site without the need of Brønsted sites or Cu dimers. In fact, the reaction scheme does not require a specific location or configuration of the Cu-ions. Similar reaction schemes containing the formation of NO<sub>2</sub> from a nitrate species to form two identical nitrite species can be constructed for Cu in 6-rings or 8-rings and also Cu dimers or other metal ions capable of one-electron redox reactions, for example, Fe zeolites, vanadium oxide, or other oxide-based catalysts.

The stoichiometry of the standard SCR reaction arises from the coupling of the two reaction cycles via the NO<sub>2</sub> that is released. The inner cycle in Scheme 1, containing the reaction of NO<sub>2</sub> with a Cu<sup>+</sup>, is, in fact, the fast SCR reaction, according to eq 2, and hence, it is intrinsically faster than the outer cycle. In this article, we refer to the steps in the inner cycle as “fast-SCR cycle” (blue arrows in Scheme 1), and the steps in the outer cycle as “NO-activation cycle” (black arrows in Scheme 1). The NO-activation cycle can be written as



Note that the NO-activation cycle includes the same reduction steps as the fast-SCR cycle.

In standard SCR, there is no excess NO<sub>2</sub>, and the rate of the fast-SCR cycle is limited by the amount of NO<sub>2</sub> available. As a result, the overall rates of the fast-SCR and NO-activation cycles become equal. The reaction steps in the NO-activation cycle are always accompanied by the reaction steps in the fast-SCR cycle at an equal rate; the result is the standard SCR reaction. It is noted that the steps in the fast-SCR cycle can occur isolated, provided NO<sub>2</sub> is available; this is the fast SCR reaction.

The total stoichiometry of the standard SCR reaction then follows from addition of the NO-activation and fast-SCR cycles in Scheme 1, and eqs 2 and 3. Ruggieri et al. have noted that the standard SCR reaction can be written as the sum of the oxidation of NO to NO<sub>2</sub>, according to  $2\text{NO} + \text{O}_2 \rightarrow 2\text{NO}_2$ , and the fast SCR reaction (eq 2).<sup>66</sup> Scheme 1 is actually a representation of that, with nitrite figuring as one of the NO<sub>2</sub> species.

The coupling of the NO-activation and fast-SCR cycles, as proposed here, has two important consequences for a fundamental understanding of the standard and fast SCR reactions. First, because the fast-SCR cycle is intrinsically faster than the outer cycle, the rate-determining step in standard SCR must involve the oxidation of NO to nitrates or nitrites or the release of NO<sub>2</sub>. The second consequence is that the chemistry of the standard SCR and fast SCR reactions essentially is the same: all reaction intermediates in the fast SCR reaction are also part of the standard SCR reaction.

It is stressed here that the reaction intermediates shown in Scheme 1 are constructed according to the requirements given above and are presented as a hypothesis at this point. Any other reaction scheme containing the element of a slow formation of NO<sub>2</sub> from NO and O<sub>2</sub> in combination with a fast-SCR step also will result in the correct stoichiometry for the SCR reaction and may be equally valid. Scheme 1 seems nevertheless reasonable because it contains the known NO<sub>3</sub><sup>-</sup>, NO<sub>2</sub><sup>-</sup>, OH<sup>-</sup>, HO–NO, and NH<sub>3</sub> ligands. The reaction path from Cu<sup>2+</sup>–OH<sup>-</sup> to Cu<sup>+</sup> consists of the same reaction steps as proposed earlier,<sup>10,51</sup> and the presence of nitrates in an SCR catalyst is also well documented.<sup>50,62,63,69,70</sup> Scheme 1 is in full agreement with the

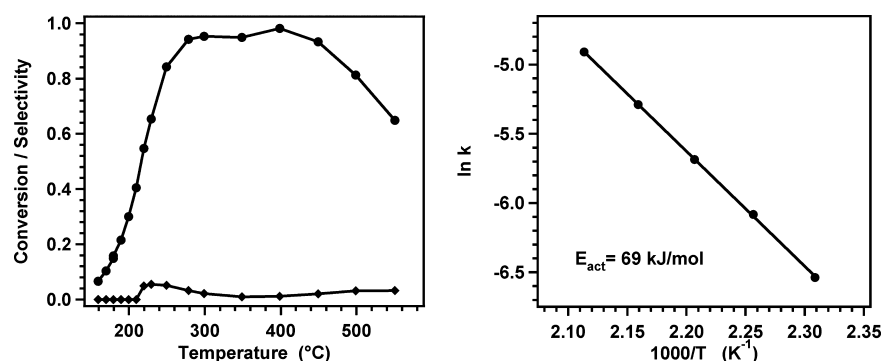


**Figure 1.** Left panel: Measured conversion of NO (circles) and selectivity to N<sub>2</sub>O (diamonds) in the temperature range 160–550 °C. Amount of catalyst: 5 mg. Feed gas: 500 ppm of NO, 533 ppm of NH<sub>3</sub>, 5% H<sub>2</sub>O, 10% O<sub>2</sub> in N<sub>2</sub>. Flow: 225 N mL/min. Right panel: Arrhenius plot of the rate constant, assuming a first-order rate equation  $r = k p_{\text{NO}}$ ; the slope corresponds to an activation energy of 69 kJ/mol.

conclusions that Cu<sup>2+</sup> is reduced by the combination of NO + NH<sub>3</sub>, followed by an oxidation by NO + O<sub>2</sub>.<sup>49</sup> A reaction between NO and nitrate to NO<sub>2</sub> has been observed in SCR over both V-based and zeolite-based catalysts,<sup>60,61</sup> and the reverse reaction releasing NO upon exposure to NO<sub>2</sub> is also known.<sup>55,62,63,71</sup> The difference between Scheme 1 and previously proposed reaction schemes does not lie in the individual reaction steps or reaction intermediates, but in the description of the standard SCR reaction as a coupling of an NO oxidation step with the fast SCR reaction via an NO<sub>2</sub> molecule.

**3.1. Verification of the Reaction Scheme.** To verify the reaction steps shown in Scheme 1 for SCR reactions, the energy profile of the NO-activation cycle at 200 °C was calculated by DFT.

Furthermore, a Cu-CHA catalyst with a Si/Al ratio of 15 and a Cu/Al ratio of 0.48, corresponding to a total Cu loading of 2.6 wt % Cu, was characterized by XAS, EPR, and FTIR. First, the reduction and oxidation steps were decoupled to obtain insight into the state of the Cu and the ligands present in these different phases of the SCR reaction, then the same techniques were also used to verify that the state of the Cu obtained by oxidation by NO and O<sub>2</sub> or by NO<sub>2</sub> was the same. Finally, the role of nitrates and nitrites and their formation by NO + O<sub>2</sub> and by NO<sub>2</sub> were studied in more detail. In all these measurements, the temperature was kept at 200 °C.

The Cu-CHA catalyst used in these characterizations is an efficient SCR catalyst. Figure 1 shows the NO conversion and N<sub>2</sub>O selectivity measured in a microreactor in the temperature range 160–550 °C. The NO conversion shows a bimodal pattern, with a first maximum around 300 °C and a second maximum around 400 °C, similar to earlier observations.<sup>39,40</sup> The decreasing NO conversion above 400 °C can be ascribed to an enhanced direct oxidation of ammonia to NO that occurs in this temperature range. It is noted that this particular Cu-CHA catalyst is very selective: N<sub>2</sub>O is the only byproduct, with a maximum selectivity of ~6% at 230 °C.

The activation energy is derived from the NO conversion data in the temperature range 160–200 °C. Assuming that the SCR reaction is first-order in NO and zeroth-order in NH<sub>3</sub>,<sup>50,56,72</sup> the rate constants for the SCR reaction at these temperatures are evaluated. From the slope of the Arrhenius plot of these data, shown in the right panel in Figure 1, an apparent activation energy of 69 kJ/mol is found, which is within the range of activation energies reported earlier.<sup>39,72</sup>

**3.1.1. Stability of Intermediates and Energy Diagram Calculated by DFT.** In each reaction step shown in Scheme 1, a molecule is adsorbed or desorbed (or both) onto or from the Cu site. The ligands on the Cu site then follow from the mass balance at each step. In the following, the stability of the different reaction intermediates as calculated by DFT is discussed to show that the proposed reaction steps in Scheme 1 are reasonable.

From DFT, we find that the most stable geometry of Cu<sup>+</sup> is in the double 6-ring and that of Cu<sup>2+</sup>–OH<sup>–</sup>, in the 8-ring, as shown in Figure 2. These two locations for the Cu ions are

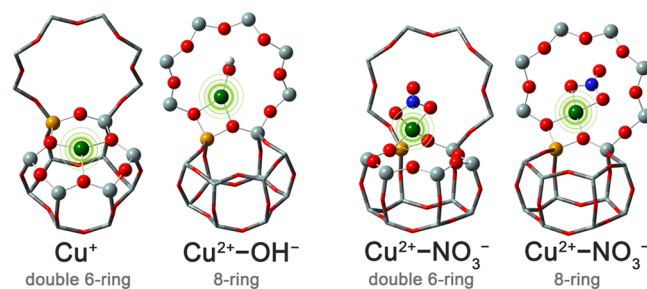


**Figure 2.** Model geometries of Cu<sup>+</sup>, Cu<sup>2+</sup>–OH<sup>–</sup>, and Cu<sup>2+</sup>–NO<sub>3</sub><sup>–</sup> in a 6-ring and an 8-ring configuration in CHA. Atoms are colored as follows: Si, gray; Al, yellow; Cu, green; N, blue; O, red; H, white.

well-known from structural analysis of Cu-CHA catalysts, although some controversy exists about which form actually constitutes the active site.<sup>6,12,28,34,39–41,44,52,72,73</sup> However, when adsorbates are present, the Cu ion is lifted out of the 6-ring plane, and the preference for the 6-ring location diminishes.<sup>42–44,74</sup> This is also observed for the formation of Cu<sup>2+</sup>–NO<sub>3</sub><sup>–</sup> (step 1), where the energy for the Cu located in the 8-ring is only 0.08 eV lower compared to the Cu in the 6-ring, showing that, in this case, there is no real preference for location of the Cu in the 6-ring or 8-ring.

The ligands in the different steps in Scheme 1 represent the most stable configuration found with DFT for the given stoichiometry; however, the order of the two consecutive adsorption steps, for example, the adsorption of NO and NH<sub>3</sub> (step 5) or NO and O<sub>2</sub> (step 1), is arbitrary because at the end, it produces the same intermediate. According to Scheme 1, the Cu<sup>2+</sup>–OH<sup>–</sup> (species E) reacts with both NH<sub>3</sub> and NO to N<sub>2</sub> and H<sub>2</sub>O, while the Cu<sup>2+</sup> is reduced to Cu<sup>+</sup>; this part is the heart of the SCR reaction. After adsorption of the NO and NH<sub>3</sub>, the stoichiometry of the ligands corresponds to that of

ammonium nitrite, and from here, a decomposition to water and nitrogen takes place. The calculated adsorption energy of NO on the  $\text{Cu}^{2+}\text{-OH}^-$  (species E) is  $-1.05$  eV to yield a  $\text{NO}^+\text{-Cu}^+\text{-OH}^-$  species and  $-1.14$  eV to yield a  $\text{Cu}^+\text{-HONO}$ -like species. These species are quite similar to the  $\text{Cu}^+\text{-NO}^+$  species proposed earlier.<sup>40,75</sup> The corresponding adsorption of  $\text{NH}_3$ , resulting in a  $\text{NH}_3\text{-Cu}^{2+}\text{-OH}^-$  species, is  $-0.93$  eV. Because these values are quite close, the actual order of adsorption of NO and  $\text{NH}_3$  seems more or less random.

An important result for the SCR reaction mechanism is that adsorption of  $\text{O}_2$  takes place on the  $\text{Cu}^+$  species. The calculated adsorption energy at 0 K of  $\text{O}_2$  on  $\text{Cu}^+$  (species A in Scheme 1) is  $-0.66$  eV. On the  $\text{Cu}^{2+}\text{-OH}^-$  ion (species E), the calculated adsorption energy is positive, and no adsorption takes place. This indicates that  $\text{O}_2$  takes part only in the reoxidation of the  $\text{Cu}^+$ .

Figure 3 shows the energy diagram of the reaction steps of the NO-activation cycle shown in Scheme 1 (black arrows).

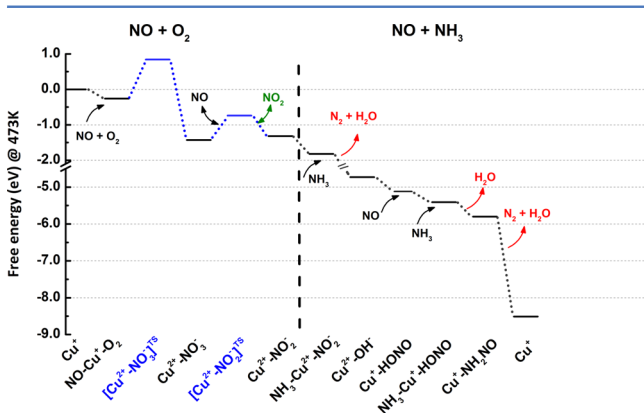


**Figure 3.** Calculated free energy diagram for the NO activation cycle shown in Scheme 1. The free energies at each level are given relative to  $\text{Z-Cu}^+$ , and the appropriate gas phase molecules. Calculated activation energies in the oxidation part are shown in blue.

The SCR reaction is strongly exothermic, and all the steps in the reduction part of the reaction, involving the reaction with  $\text{NH}_3$  and NO, are exothermic, which is consistent with a fast and effective reduction of the  $\text{Cu}^{2+}\text{-OH}^-$  (species E) to the  $\text{Cu}^+$  (species A) in a mixture of NO and  $\text{NH}_3$ . In the oxidation part of the reaction, the adsorption of  $\text{NO} + \text{O}_2$  and formation

of the nitrate are exothermic, but the formation of nitrite under the release of  $\text{NO}_2$  (step 2) is endothermic. This is an indication that this reaction step is an equilibrium reaction, which is consistent with earlier reports that this reaction can occur in both directions.<sup>55,62,63</sup>

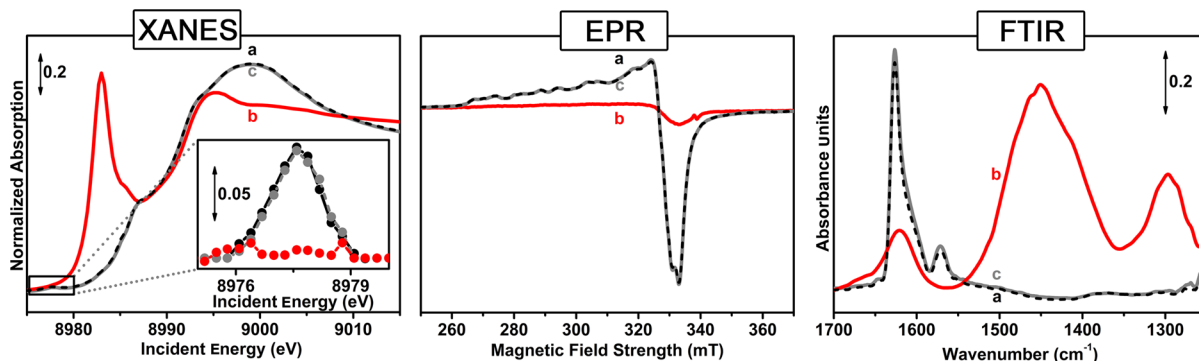
As noted above, the rate-determining step of the standard SCR reaction is the oxidation of NO to nitrates (step 1) or the release of  $\text{NO}_2$  (step 2). The calculated activation energies for these steps are 1.08 eV for the nitrate formation and 0.67 eV for the release of  $\text{NO}_2$  (Figure 3). This indicates that the oxidation of NO with  $\text{O}_2$  to a  $\text{Cu}^{2+}$  nitrate species is the rate-determining step of the standard SCR reaction.

The calculated activation energy of 1.08 eV is somewhat higher than the measured apparent activation energy of 69 kJ/mol (0.72 eV); the experimental value probably includes other factors, such as the adsorption energy of the reactants as described by the Langmuir isotherm, which have not been taken into account in the DFT calculation.

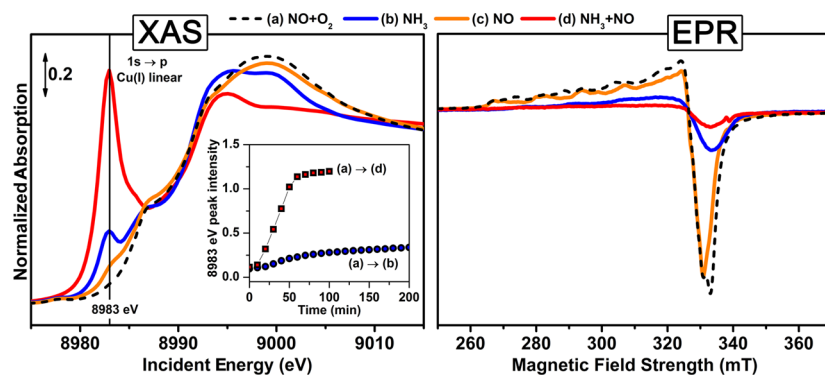
**3.1.2. Characterization of Cu-CHA in Decoupled Oxidation and Reduction.** According to Scheme 1, it should be possible to perform the oxidation and reduction parts of the SCR reaction separately by exposing the catalyst alternately to a mixture containing NO and  $\text{O}_2$  and a mixture containing  $\text{NH}_3$  and NO. To verify Scheme 1, we follow the state of the catalyst in situ after oxidation in  $\text{NO} + \text{O}_2$ , reduction in  $\text{NH}_3 + \text{NO}$ , and again oxidation in  $\text{NO} + \text{O}_2$  by XAS, EPR, and FTIR. These oxidation and reduction steps constitute a complete catalytic cycle, and therefore, the second oxidation step should restore the original state of the catalyst.

Figure 4 shows the Cu K-edge XAS spectrum in the XANES (X-ray absorption near edge structure) region, EPR, and FTIR for the Cu-CHA catalyst after initial oxidation in  $\text{NO} + \text{O}_2$ , after reduction in  $\text{NH}_3 + \text{NO}$ , and after reoxidation in  $\text{NO} + \text{O}_2$ . All results clearly indicate that the state of the Cu after reoxidation is identical to that obtained after initial oxidation, indicating that the reduction and oxidation steps as performed here constitute a catalytic cycle.

The XANES and EPR spectra also provide evidence that the oxidation state changes from  $\text{Cu}^{2+}$  to  $\text{Cu}^+$  during the exposure to  $\text{NH}_3$  and NO together. In particular, the XANES spectrum measured after reduction in  $\text{NH}_3 + \text{NO}$  (curve b) is characterized by an intense pre-edge peak at  $\sim 8983$  eV due to the  $1s \rightarrow 4p$  transitions in  $\text{Cu}^+$  compounds with a low coordination number.<sup>44,76</sup> Furthermore, the weak pre-edge



**Figure 4.** In situ XAS (left panel), EPR (middle panel), and FTIR (right panel) spectra collected during reduction and oxidation in SCR over of Cu-CHA (2.6 wt % Cu) at 200 °C in the following consecutive steps: (a) initial oxidation in 1000 ppm of  $\text{NO}/10\%$   $\text{O}_2$  (dashed black curves); (b) reduction in 1200 ppm of  $\text{NH}_3/1000$  ppm of NO (solid red curve); (c) reoxidation in 1000 ppm of  $\text{NO}/10\%$   $\text{O}_2$  (solid gray curve). Inset left panel: background-subtracted XANES pre-edge peak, characteristic for the  $\text{Cu}^{2+}$   $1s \rightarrow 3d$  transition, indicating the presence of  $\text{Cu}^{2+}$ .



**Figure 5.** In situ XANES at the Cu K-edge (left panel) and EPR (right panel) showing the reducing capability at 200 °C of 1200 ppm of NH<sub>3</sub> (b: solid blue curve), 1000 ppm of NO (c: solid orange curve), and a mixture of 1200 ppm of NH<sub>3</sub> and 1000 ppm of NO (d: solid red curve) on the Cu(II) state obtained after initial oxidation in a mixture of 1000 ppm of NO and 10% O<sub>2</sub> (a: dashed black curve). Inset left panel: Development of the intensity at 8983 eV with time with NH<sub>3</sub> only (a → b) and with a mixture of NH<sub>3</sub> + NO (a → d), visualizing the different reduction behavior with time in these cases. In EPR, a stable state is obtained after 11 min in NH<sub>3</sub> + NO (red), whereas the EPR spectra are still developing after 11 min in NH<sub>3</sub> alone (blue) or 30 min in NO (orange).

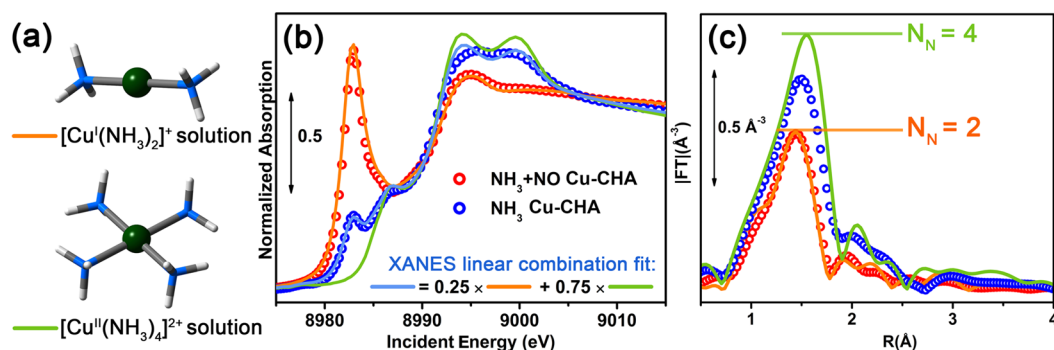


**Figure 6.** (a) The linear [Cu<sup>I</sup>(NH<sub>3</sub>)<sub>2</sub>]<sup>+</sup> and square planar [Cu<sup>II</sup>(NH<sub>3</sub>)<sub>4</sub>]<sup>2+</sup> complexes: Cu, green; N, blue; H, white. (b) Cu K-edge XANES spectra and (c) *k*<sup>2</sup>-weighted, phase uncorrected Fourier transformed EXAFS in the *k* range 2.4–12.4 Å<sup>-1</sup> of the Cu-amino complexes (orange and green solid lines) compared with the data for Cu-CHA exposed to 1200 ppm of NH<sub>3</sub> and 1200 ppm of NH<sub>3</sub>/1000 ppm of NO at 200 °C (empty circles). Panel (b) also shows that the spectrum for Cu-CHA reduced in 1200 ppm of NH<sub>3</sub> corresponds to a linear combination of 25% [Cu<sup>I</sup>(NH<sub>3</sub>)<sub>2</sub>]<sup>+</sup> and 75% [Cu<sup>II</sup>(NH<sub>3</sub>)<sub>4</sub>]<sup>2+</sup> (light blue solid line). The data indicate that Cu is mostly reduced to Cu<sup>+</sup> in a mixture of NO and NH<sub>3</sub> at 200 °C, whereas the majority of Cu remains in the Cu<sup>2+</sup> state when exposed to NH<sub>3</sub>.

peak at ~8978 eV, which is a fingerprint of the 1s → 3d transition in Cu<sup>2+</sup>,<sup>54,77–81</sup> has disappeared (inset in Figure 4, left panel). In EPR (Figure 4, middle panel), the signal intensity relative to the total Cu content decreases from 0.59 to 0.18. (the signal intensities have been corrected according to the Boltzmann equation). This indicates that a significant part of the Cu changes from an EPR active Cu<sup>2+</sup> to the EPR-silent Cu<sup>+</sup> state. This change in oxidation state is in line with Scheme 1 and reaction schemes published earlier.<sup>9,10,49,51</sup> The EPR active species that constitutes the difference between the dashed and the orange curves in Figure 4 has the spin Hamiltonian parameters  $g_{\parallel} = 2.28$  and  $A_{\parallel} = 449$  MHz, which can be assigned to a Cu<sup>2+</sup> nitrate species.<sup>82</sup>

The FTIR spectra in Figure 4 (right panel) after initial NO + O<sub>2</sub> exposure (curve a) reveal the appearance of IR bands at 1627(s), 1607(sh), and 1570(w) cm<sup>-1</sup>; all three bands are associated with NO<sub>3</sub><sup>-</sup> coordinated to Cu sites.<sup>69</sup> The nitrate bands promptly disappear upon interaction with the NO + NH<sub>3</sub> mixture, and the final spectrum (curve b) is dominated by bands related to strongly adsorbed NH<sub>3</sub> species. In particular, bands at 1620 and 1297 cm<sup>-1</sup> are associated with asymmetric and symmetric N–H bending vibration of molecular NH<sub>3</sub> adsorbed on Cu sites, respectively. The frequencies of these modes found by DFT are 1640 and 1321 cm<sup>-1</sup>, in agreement

with the experimental values. The bending N–H vibration of NH<sub>3</sub> adsorbed on Brønsted sites in form of NH<sub>4</sub><sup>+</sup> ions shows a maximum at 1460 cm<sup>-1</sup>.<sup>83</sup> The complete disappearance of these bands upon NO + O<sub>2</sub> exposure and final restoration of the initial state dominated by Cu nitrate features (curve c) prove the reoxidation and closes the SCR cycle.

Following Scheme 1, the reduction of Cu<sup>2+</sup> to Cu<sup>+</sup> requires both NH<sub>3</sub> and NO. As a consequence, the reduction should result in different states of the Cu, if one of these components is missing. This is confirmed by the results reported in Figure 5, which shows XANES spectra at the Cu K-edge and EPR for Cu-CHA in the presence of NO or NH<sub>3</sub> alone at 200 °C, together with that obtained in the presence of both NO and NH<sub>3</sub>.

The XANES spectra clearly show that exposure to NO alone at 200 °C essentially leads to a Cu<sup>2+</sup> state that is similar to the Cu<sup>2+</sup> obtained with oxidation in a mixture of NO and O<sub>2</sub>. This indicates that interaction with NO alone does not result in significant reduction of the Cu<sup>2+</sup> species at this temperature. In EPR, exposure to NO alone leads to an EPR spectrum that is identical to that obtained with dehydrated Cu-CHA.<sup>29</sup> Upon oxidation with NO and O<sub>2</sub>, however, a difference is observed, indicating that an additional Cu species is formed in this case. This suggests that a fully oxidized Cu<sup>2+</sup> species in the 6-ring is

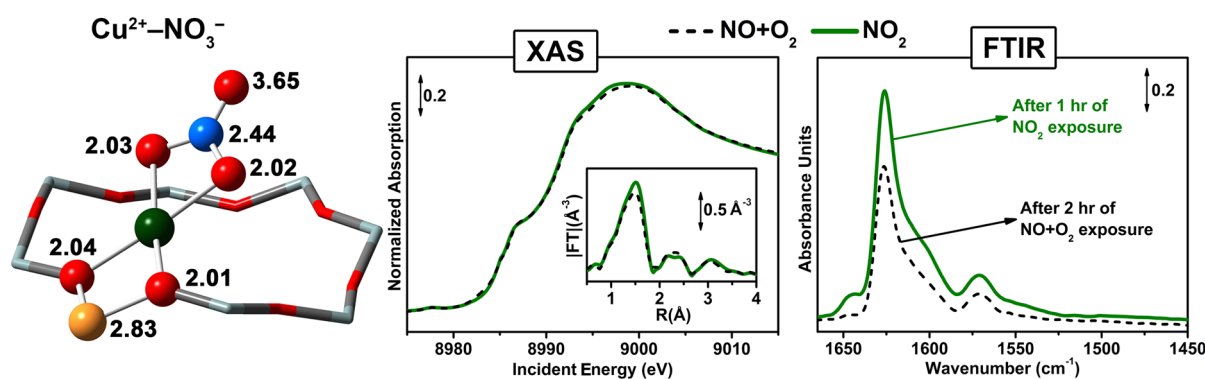


**Figure 7.** Structure of the bidentate Cu-NO<sub>3</sub><sup>-</sup> species (left panel). In situ XAS and  $k^2$ -weighted, phase uncorrected Fourier transformed EXAFS (middle panel) and FTIR (right panel) spectra after exposure of dehydrated Cu-CHA to 1000 ppm of NO<sub>2</sub> (solid green curves), and to a mixture of 1000 ppm of NO and 10% O<sub>2</sub> (dashed black curves) at 200 °C. The left panel indicates the distances from the central Cu atom to the neighboring atoms in angstroms. Color code atoms: Cu, green; O, red; N, blue; Al, yellow.

obtained in both cases, but that oxidation in the mixture of NO and O<sub>2</sub> also produces a Cu<sup>2+</sup> species that is not located in the 6-ring.

In the presence of NH<sub>3</sub> alone, the pre-edge peak at ~8983 eV, which is characteristic for a Cu<sup>+</sup> species, is remarkably less pronounced compared with that obtained with the mixture of NO and NH<sub>3</sub>, and it develops much more slowly (see inset Figure 5, left panel). This indicates that the combination of NO and NH<sub>3</sub> results in a different state of the Cu, compared with the state obtained upon exposure to NO or NH<sub>3</sub> alone, in good agreement with previous results.<sup>49,51</sup> In EPR, exposure to NH<sub>3</sub> alone at 200 °C leads to a decrease in the signal intensity, in 11 min, to 29% relative to the total amount of Cu and a further decrease to 19% in about 3 h. In a mixture of NO and NH<sub>3</sub>, the EPR signal decreases to 18% in 11 min, clearly showing that the reduction is faster in this case. These results indicate that the NO/NH<sub>3</sub> mixture acts as a different, more powerful reducing agent that is essential in the reducing part of the SCR reaction.

**3.1.3. Identification of the Cu<sup>+</sup> and Cu<sup>2+</sup> States.** A more detailed analysis of the XAS and FTIR data in Figures 4 and 5 provides information on the identity of the Cu<sup>+</sup> and Cu<sup>2+</sup> species. In Figure 6, we compare the in situ XAS spectra of Cu-CHA in the presence of NH<sub>3</sub> only and NH<sub>3</sub> + NO, shown in Figure 5, with those for the linear [Cu<sup>I</sup>(NH<sub>3</sub>)<sub>2</sub>]<sup>+</sup> and square planar [Cu<sup>II</sup>(NH<sub>3</sub>)<sub>4</sub>]<sup>2+</sup> amino complexes in solution, which have been measured as a reference. The XAS spectrum of the Cu-CHA zeolite after reduction in the NH<sub>3</sub> + NO mixture at 200 °C is almost identical to that of the linear [Cu<sup>I</sup>(NH<sub>3</sub>)<sub>2</sub>]<sup>+</sup> complex, both in the XANES and in the EXAFS regions. This provides strong evidence for a substantial reduction of the Cu in the catalyst to a Cu<sup>+</sup> state and reveals that the Cu is predominantly present as a [Cu<sup>I</sup>(NH<sub>3</sub>)<sub>2</sub>]<sup>+</sup> complex after reduction in a mixture of NO and NH<sub>3</sub> at 200 °C. As judged from the Cu-N coordination number of ~2 in the first shell (see panel c in Figure 6) and the lack of a second shell contribution associated with the Cu-Si or Cu-Al coordination,<sup>28,52</sup> the Cu is only weakly bound to the zeolite. This suggests that the Cu is mobile, even at 200 °C. It is noted that the linear [Cu<sup>I</sup>(NH<sub>3</sub>)<sub>2</sub>]<sup>+</sup> complex is not specifically mentioned in Scheme 1, but it can be regarded as NH<sub>3</sub> adsorbed on Cu<sup>+</sup>.

After reduction with NH<sub>3</sub> alone, the intensity at 8983 eV in the Cu K-edge XANES spectrum remains lower than that obtained after reduction in a mixture of NO and NH<sub>3</sub> (see Figure 5). In Figure 6, this spectrum is compared to those for

the [Cu<sup>I</sup>(NH<sub>3</sub>)<sub>2</sub>]<sup>+</sup> and [Cu<sup>II</sup>(NH<sub>3</sub>)<sub>4</sub>]<sup>2+</sup> amino-complexes, as well. The measured XANES spectrum is well reproduced, with a contribution of ~75% of the square-planar [Cu<sup>II</sup>(NH<sub>3</sub>)<sub>4</sub>]<sup>2+</sup> complex and 25% of the linear [Cu<sup>I</sup>(NH<sub>3</sub>)<sub>2</sub>]<sup>+</sup> complex. This clearly indicates that a majority of the Cu species is present as Cu<sup>2+</sup> and, therefore, is not reduced by NH<sub>3</sub> alone at 200 °C, confirming the conclusion that the mixture of NH<sub>3</sub> and NO is a stronger reducing agent than NH<sub>3</sub> alone. The first-shell coordination number in this case is between 2 and 4, as expected for a mixture of [Cu<sup>II</sup>(NH<sub>3</sub>)<sub>4</sub>]<sup>2+</sup> and [Cu<sup>I</sup>(NH<sub>3</sub>)<sub>2</sub>]<sup>+</sup> complexes.

The reaction scheme also postulates that oxidation of Cu<sup>+</sup> by NO + O<sub>2</sub> or NO<sub>2</sub> leads to identical Cu species. Earlier in this section, we identified these species by FTIR and EPR spectroscopy as nitrates on Cu<sup>2+</sup> (Figure 4). Figure 7 (right panel) shows that the same set of vibrational bands is observed after oxidation of the Cu<sup>+</sup> species in a mixture of NO and O<sub>2</sub> or NO<sub>2</sub>. The higher overall intensity of this set of bands obtained with only NO<sub>2</sub> in the gas feed indicates that nitrate formation is more efficient in this case. Figure 7 (middle panel) shows that the Cu K-edge XANES and Fourier transformed EXAFS spectra for the Cu<sup>2+</sup> state obtained by oxidation in NO/O<sub>2</sub> or NO<sub>2</sub> are identical, thus confirming that oxidation of Cu<sup>+</sup> by NO + O<sub>2</sub> or NO<sub>2</sub> leads to the same Cu<sup>2+</sup> species.

A more detailed EXAFS analysis after oxidation of the Cu-CHA in an NO/O<sub>2</sub> mixture reveals the structure of the nitrate species (Figure 7, middle panel). It is important to note that the Fourier transformed EXAFS does not show a significant contribution in the 2.8–3.0 Å range, which is typical for the Cu-Cu distance, indicating a predominantly monomeric Cu species. The maximum in the Fourier transformed EXAFS spectrum at ~2.5 Å indicates a contribution of a Si or Al atom of the zeolite framework, which means that the Cu is bound to the zeolite framework. These features rule out a bridging nitrate configuration between neighboring Cu<sup>2+</sup> ions, in agreement with previous studies.<sup>27,28</sup> A number of different configurations for the nitrate species were optimized by DFT and tried in the EXAFS analysis, and by far, the best agreement with the EXAFS data was obtained with a chelating bidentate nitrate on a single Cu<sup>2+</sup> site, close to 1 Al atom. This structure is shown in Figure 7, left panel, and is also indicated in Scheme 1, species B. DFT calculations also show that the bidentate configuration of the nitrate group on the Cu<sup>2+</sup> site is the most stable. The feature around 3 Å in the Fourier transformed EXAFS corresponds to a

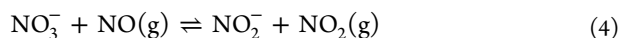


coordination geometry around the Cu center that is very specific for a bidentate nitrate species. The DFT calculations of the chelating bidentate nitrate ligand also reveal a vibrational mode at  $1570\text{ cm}^{-1}$  associated with the stretching mode of the N=O bond that points away from the Cu ion. Consequently, the vibrational bands at  $1627(\text{s})$ ,  $1607(\text{sh})$ , and  $1570(\text{w})\text{ cm}^{-1}$  in the FTIR spectrum, observed after oxidation in NO/O<sub>2</sub> or NO<sub>2</sub>, correspond to a chelating bidentate nitrate configuration on a monomeric Cu species.<sup>63,69,75</sup>

#### 4. THE NITRATE–NITRITE EQUILIBRIUM

From the discussion above, we find that the Cu<sup>2+</sup> species formed upon reaction of a Cu<sup>+</sup> with NO + O<sub>2</sub> or NO<sub>2</sub> is a bidentate nitrate species (Cu<sup>2+</sup>–NO<sub>3</sub><sup>−</sup>, species B). According to Scheme 1, the reaction of NO<sub>2</sub> with the Cu<sup>+</sup> should result in a nitrite species; however, as mentioned above, step 2 in Scheme 1 is an equilibrium reaction,<sup>63</sup> and consequently, an exposure of Cu<sup>+</sup> to NO<sub>2</sub> results in the formation of a nitrate species<sup>55,59,63,64</sup> under the release of NO. To understand why generally nitrate species are found in an in situ measurement of Cu-CHA, we consider the equilibrium between nitrates and nitrites (step 2) and the formation of NO<sub>2</sub> in the gas phase.

The equilibrium between nitrates and nitrites can be written as follows (step 2):



The equilibrium constant,  $K$ , associated with the equilibrium reaction in eq 4 is written as

$$K = \frac{p_{\text{NO}_2}}{p_{\text{NO}}} \quad (5)$$

where  $p_{\text{NO}_2}$  and  $p_{\text{NO}}$  are the partial pressures of NO<sub>2</sub> and NO, respectively. To calculate the value of the equilibrium constant in eq 5, the standard Gibbs free energy ( $\Delta G^0$ ) of the equilibrium reaction is estimated using the tabulated values for the Gibbs free energy of formation<sup>84</sup> ( $\Delta G_f^0$ ) for alkali nitrates, the corresponding nitrites, NO, and NO<sub>2</sub>.<sup>85</sup> At 200 °C,  $\Delta G^0$  is found to be +40 to +50 kJ/mol, which corresponds to an equilibrium constant of  $3.0 \times 10^{-6}$  to  $3.8 \times 10^{-5}$ . With a NO concentration of 500 ppm in the gas, this corresponds to equilibrium concentrations of NO<sub>2</sub> in the range 2–20 ppb. The formation of nitrite and NO<sub>2</sub> by reaction with NO will occur only if the concentration of NO<sub>2</sub> is below the equilibrium concentration; otherwise, the reaction proceeds in the other direction.

The low value of the equilibrium constant implies that the steady-state concentration of NO<sub>2</sub> in the SCR reaction must be low for the reaction to proceed. In the SCR reaction, NO<sub>2</sub> reacts according to the fast-SCR reaction, eq 2, and the higher rate of that reaction compared to the standard SCR reaction can ensure such a low steady-state concentration. A steady-state concentration of this magnitude and the corresponding low concentration of the nitrite species are difficult to determine experimentally in in situ measurements.

Another consequence of the very low equilibrium concentrations of NO<sub>2</sub> is that the equilibrium shifts to the nitrate side, already at concentrations well below 1 ppm. In most experimental setups, some NO<sub>2</sub> will always be present in mixtures of NO and O<sub>2</sub> because of the oxidation of NO to NO<sub>2</sub> in the gas phase. The kinetics of this reaction are well-known from atmospheric chemistry.<sup>86</sup> Using a third order rate law  $r = k c_{\text{NO}}^2 c_{\text{O}_2}$  and the rate constant  $k$  (in  $\text{L mol}^{-2} \text{s}^{-2}$ ) given by

$k = 1.2 \times 10^3 e^{530/T}$  ( $T$  is the temperature in K),<sup>86</sup> it is calculated that it takes only a few seconds to produce 2–20 ppb NO<sub>2</sub> in a mixture of 500 ppm of NO and 10% oxygen at 200 °C. This means that, in practice, a mixture of NO and O<sub>2</sub> contains an amount of NO<sub>2</sub> that is higher than the estimated equilibrium concentration, and hence, the equilibrium is usually shifted toward the nitrates in the presence of NO and O<sub>2</sub>. It is noted that the gas phase oxidation of NO to NO<sub>2</sub> is several orders of magnitude slower than the catalytic SCR reaction, which is capable of converting a few hundred parts per million of NO in milliseconds. Therefore, the contribution of the gas phase oxidation of NO to NO<sub>2</sub> in the SCR reaction is negligible.

When there is no oxygen present in the gas phase, then the concentration of NO<sub>2</sub> can become low enough to shift the equilibrium in eq 4 toward the nitrite side and observe a transient release of NO<sub>2</sub> upon exposure of the nitrate phase to NO.<sup>62,64</sup> This effect is also shown in Figure 8, which shows the

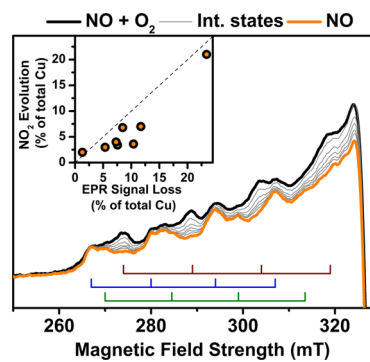


**Figure 8.** EPR of Cu-CHA after exposure to NO/O<sub>2</sub> at 200 °C (black) and the transformation in the first 30 min after the O<sub>2</sub> has been removed. The final spectrum is shown in orange. The sets of lines corresponding to three different Cu<sup>2+</sup> species are shown: The two persistent sets (green and blue) correspond to two different Cu<sup>2+</sup> sites in the 6-ring. The set that disappears (brown) corresponds to the Cu<sup>2+</sup>–NO<sub>3</sub><sup>−</sup> species. Inset: Transient amount of NO<sub>2</sub> formed compared with the quantified loss of EPR signal intensity for eight independent experiments on fresh and reused Cu-CHA samples.

changes in the EPR signal of the Cu-CHA catalyst when the oxygen is removed from a 1000 ppm of NO/10% O<sub>2</sub> mixture. The difference between the orange and black spectrum in Figure 8 corresponds to a tetragonal Cu<sup>2+</sup> species with parallel spin Hamiltonian parameter values  $g_{\parallel} = 2.28$  and  $A_{\parallel} = 449$  MHz. These values are close to those for the Cu species found after adsorption of NO<sub>2</sub> on Cu-MFI,  $g_{\parallel} = 2.29$  and  $A_{\parallel} = 462$  MHz, and assigned to a Cu<sup>2+</sup> nitrate species.<sup>82</sup> This shows that the Cu<sup>2+</sup>–NO<sub>3</sub><sup>−</sup> species reacts with NO. Upon removing the O<sub>2</sub>, a transient formation of NO<sub>2</sub> is observed, and the amount of this NO<sub>2</sub> correlates to the amount of EPR active species that disappears when the O<sub>2</sub> is removed (see Figure 8).

Because we observe only the disappearance of the EPR signal with  $g_{\parallel} = 2.28$  and not the development of a new feature, it is concluded that the Cu-nitrite Cu<sup>2+</sup>–NO<sub>2</sub><sup>−</sup> is EPR-inactive. The remaining species (orange curve in Figure 8) is similar to that observed after dehydration of a Cu-CHA catalyst.<sup>29</sup> These EPR signals, corresponding to Cu<sup>2+</sup> in 6-ring sites are persistent and are present both in an atmosphere of only NO and in a mixture of NO and O<sub>2</sub> at 200 °C. This indicates that the Cu<sup>2+</sup> 6-ring sites do not form nitrates under the experimental conditions used in this EPR experiment.

## 5. NO OXIDATION AS RATE-DETERMINING STEP IN STANDARD SCR

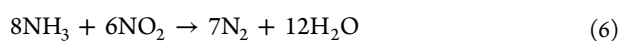
In Scheme 1, we have identified the oxidation of NO to nitrate as the rate-determining step of the standard SCR reaction. This contradicts the conclusions of Ruggeri et al., who ruled out the NO oxidation as the rate-determining step for the SCR reaction, on the basis of the very low rate of NO oxidation on a Cu zeolite.<sup>66</sup> These opposing conclusions can be reconciled by realizing that the NO oxidation reaction over a Cu zeolite is also the result of a complete catalytic cycle and not of a single reaction step. The NO oxidation part in Scheme 1 does not represent a complete catalytic cycle because the oxidation state of the Cu changes from Cu<sup>+</sup> to Cu<sup>2+</sup>, and therefore, this part alone does not correctly represent the catalytic oxidation of NO to NO<sub>2</sub> over a Cu zeolite.

If we assume that the catalytic oxidation of NO to NO<sub>2</sub> takes place on a Cu<sup>+</sup> site, as is the case in the SCR reaction, then the formation of NO<sub>2</sub> is accompanied by an oxidation of the Cu<sup>+</sup> to Cu<sup>2+</sup>; however, the reduction of this Cu<sup>2+</sup> to Cu<sup>+</sup> will be much slower than in the SCR reaction because there is no possibility for the very efficient reduction with NH<sub>3</sub> and NO in the catalytic oxidation of NO to NO<sub>2</sub>. This is supported by the XANES results (Figure 4, left panel), which show only a Cu<sup>2+</sup> species (no Cu<sup>+</sup> species) in the Cu-CHA in the presence of NO and O<sub>2</sub>. This means that the oxidation of NO in the absence of NH<sub>3</sub> is limited by a slow reduction of Cu<sup>2+</sup> to Cu<sup>+</sup>, whereas the SCR reaction is limited by the NO oxidation to nitrate. This is a first explanation how a Cu zeolite can be a good catalyst for SCR, but a poor catalyst for the oxidation of NO to NO<sub>2</sub>, even though the NO oxidation is the rate-determining step in the standard SCR reaction.

A second explanation is that NO oxidation in the absence of NH<sub>3</sub> proceeds via a pathway entirely different from that depicted in Scheme 1. In fact, the low equilibrium concentration of NO<sub>2</sub> in the transition from nitrate to nitrite species (step 2), as estimated above, would actually limit the possible yield of NO<sub>2</sub> to a very low level. This suggests that NO oxidation in the absence of NH<sub>3</sub> cannot proceed in this way. Following this argument, the oxidation of NO to NO<sub>2</sub> in the absence of NH<sub>3</sub> is different from the NO oxidation step in the standard SCR reaction. The rates of NO oxidation in the absence and presence of NH<sub>3</sub> (SCR) then become different, and therefore, no conclusion on the NO oxidation rate in SCR can be made on the basis of measurements of NO oxidation in the absence of NH<sub>3</sub>. The conclusion that the oxidation of NO to NO<sub>2</sub> requires a Cu dimer but the SCR reaction can proceed on a single Cu-ion is a good illustration of this scenario.<sup>12,36</sup>

## 6. STANDARD SCR, FAST SCR, AND SLOW SCR

From Scheme 1, it follows that NO is required in both the oxidation and the reduction part of the SCR reaction. However, NO<sub>2</sub> can also be reduced by NH<sub>3</sub> to produce N<sub>2</sub> and H<sub>2</sub>O in the absence of NO, according to



This reaction is slower than the fast and standard SCR reactions and is known as "slow SCR" reaction. On the basis of Scheme 1, it is straightforward to understand the chemistry that controls the rate of the standard, fast, and slow SCR reactions. The rate of the standard SCR reaction is controlled by the oxidation of NO to NO<sub>2</sub>. In fast SCR, this rate-determining

step is bypassed, which explains why the fast SCR is faster than the standard SCR.

NO plays a dual role in the standard SCR reaction: it is required both for the oxidation of Cu<sup>+</sup> to Cu<sup>2+</sup> and for the reduction of Cu<sup>2+</sup> to Cu<sup>+</sup>, together with NH<sub>3</sub>. In fast SCR, NO is no longer required for the oxidation part, but it is still needed for the reduction of the Cu<sup>2+</sup> species. This is the reason why the fast SCR also requires NO, and according to Scheme 1, the optimal conditions are obtained for equimolar amounts of NO and NO<sub>2</sub>.

In the slow SCR reaction, eq 6, the fast reduction of Cu<sup>2+</sup> cannot occur because NO is not available. Consequently, the slow SCR reaction involves different reaction steps and reaction intermediates for the reduction of Cu<sup>2+</sup> to Cu<sup>+</sup>, which apparently are slower. This implies that the chemistry of the slow SCR reaction is actually different from that of the standard and fast SCR reactions. The fact that the slow SCR reaction is slower also illustrates the importance of NO for the reduction part of the standard and fast SCR reactions.

## 7. ROLE OF CU DIMERS AND BRØNSTED SITES

According to Scheme 1, the SCR reaction does not require the presence of Cu dimers or Brønsted sites. All reaction intermediates are accommodated on isolated Cu ions, and the calculated stability of the intermediates (Figure 3) seems sufficient for the reaction to occur in such a way. This is consistent with a constant activity per Cu atom.<sup>47</sup> Nevertheless, the formation of Cu dimers can still be beneficial for the SCR reaction. Measurements actually show an increase in the activity per Cu site with increasing Cu loading for SCR over Cu-SSZ-13 catalysts.<sup>39,40</sup> Because the propensity for Cu dimer formation increases with Cu loading, this may indicate that Cu dimers could enhance the rate of the NH<sub>3</sub>-SCR reaction. A possible scenario is that the oxygen leaves a single O atom on each Cu ion. Then, the rate-limiting nitrate formation in Scheme 1 could be circumvented according to  $2\text{Cu}^+ + 2\text{NO} + \text{O}_2 \rightarrow 2\text{NO}_2^- - \text{Cu}^{2+}$ , leading to a faster SCR reaction.

The effect of Brønsted sites on the SCR reaction is limited.<sup>12,22</sup> As adsorption sites for ammonia, Brønsted sites may influence the SCR reaction by an interaction with neighboring Cu-species. The conclusions that Brønsted sites promote the SCR reaction in Fe zeolite catalysts<sup>23</sup> and that the SCR activity of Cu-SAPO-34 catalysts increases proportionally with acid density seem to support such an influence. An interesting observation is that pairs of NH<sub>4</sub><sup>+</sup> in H-ZSM-5 and mordenite zeolites show SCR activity with NO<sub>2</sub>(g) species.<sup>3</sup> In Scheme 1, this would imply that Brønsted sites can contribute to the activity of the fast SCR cycle. Because the fast SCR cycle is also a part of the standard SCR reaction, Brønsted sites may influence the standard SCR reaction in this way.

## 8. CONCLUSIONS

For the first time, a consistent reaction scheme for the complete catalytic cycle of the standard and fast SCR reactions is presented. The reaction scheme describes the standard SCR reaction cycle as a coupling of an NO oxidation step to the fast SCR reaction, running at equal rates. This leads to the correct stoichiometry for the standard SCR reaction while the mass and charge balances are maintained in each step. The coupling is made by the release of an NO<sub>2</sub> molecule in a reaction of NO with a nitrate species, leaving a nitrite species at the catalytic

site. The NO<sub>2</sub> molecule that is released forms an identical nitrite species elsewhere in the catalyst.

The reaction scheme shows that it is conceivable that the SCR reaction proceeds on a single Cu-ion in the zeolite without the need for Cu dimer formation or interaction with Brønsted acidic sites.

The reaction scheme has been corroborated experimentally in three ways, using a Cu-CHA catalyst. First, a reduction in a mixture of NO and NH<sub>3</sub> followed by oxidation in a mixture of NO and O<sub>2</sub> restores the original state of the catalyst, showing that these steps constitute a catalytic cycle. Second, the same bidentate nitrate species (Cu–NO<sub>3</sub><sup>−</sup>) is formed upon exposure of the Cu<sup>+</sup> state to a mixture of NO and O<sub>2</sub> or to NO<sub>2</sub>, which confirms that the standard and fast SCR reactions follow the same scheme. Finally, the reduction of Cu<sup>2+</sup> to Cu<sup>+</sup> requires the presence of both NH<sub>3</sub> and NO. The product of this reduction is a weakly bound [Cu<sup>I</sup>(NH<sub>3</sub>)<sub>2</sub>]<sup>+</sup> linear species, which can be regarded as a Cu<sup>+</sup> covered with NH<sub>3</sub>. A reaction of the Cu<sup>2+</sup> state with NH<sub>3</sub> alone leads primarily to a [Cu<sup>II</sup>(NH<sub>3</sub>)<sub>4</sub>]<sup>2+</sup> complex. Exposure of the Cu<sup>2+</sup> to NO alone at 200 °C does not lead to a measurable reduction of the Cu.

All reaction steps are exothermic, except the formation of a Cu<sup>2+</sup> nitrite by reaction of NO with Cu<sup>2+</sup> nitrate. The latter reaction is an equilibrium reaction that depends on the partial pressures of NO and NO<sub>2</sub>. Under typical conditions for SCR, the equilibrium partial pressure of NO<sub>2</sub> is on the order of 2–20 ppb, indicating that the steady-state partial pressure of NO<sub>2</sub> in SCR is very low. As gas phase oxidation of NO and O<sub>2</sub> can produce such amounts of NO<sub>2</sub> in a few seconds; nitrate species are typically observed in mixtures of NO and O<sub>2</sub>, as well.

All reaction steps involved in the fast SCR reaction are also part of the standard SCR reaction. As a consequence, the rate-determining step must involve the oxidation of NO by O<sub>2</sub>; a density functional theory calculation of the activation energies in a Cu-CHA points to the formation of a bidentate nitrate (Cu–NO<sub>3</sub><sup>−</sup>) species as the rate-determining step.

To resolve the apparent contradiction that the oxidation of NO by O<sub>2</sub> is rate-determining in the standard SCR reaction over a Cu zeolite and such catalysts have a much lower activity for the oxidation of NO to NO<sub>2</sub>, it is realized that the rates of the SCR and NO oxidation reactions are the result of two different catalytic cycles. In the absence of NH<sub>3</sub>, the reduction of Cu<sup>2+</sup> to Cu<sup>+</sup> cannot occur in the same way as in the SCR reaction, and the reduction of Cu<sup>2+</sup> to Cu<sup>+</sup> becomes rate-determining in the oxidation of NO to NO<sub>2</sub>. Alternatively, the oxidation of NO to NO<sub>2</sub> follows a reaction path that does not involve a Cu<sup>+</sup> species.

## 9. EXPERIMENTAL SECTION

The Cu-CHA sample was prepared using a method similar to that reported earlier.<sup>27</sup> A synthesis gel with the composition 1.0 SiO<sub>2</sub>/0.0667 Al/0.5 TMAdaOH/0.5 HF/3 H<sub>2</sub>O was prepared by dissolving aluminum isopropoxide (98%, Sigma-Aldrich) in tetraethyl orthosilicate (98% Aldrich) and adding N,N,N-trimethyladamantammonium hydroxide (TMAdaOH, 25 wt %, Sachem) to the solution. This mixture was stirred to homogenize overnight. Hydrofluoric acid (48 wt %, 99.99% trace-metal basis, Sigma-Aldrich) was added, and the mixture was stirred by hand. Water was evaporated from the gel at 60 °C under regular homogenization by hand until the desired content was obtained. To form the CHA zeolite, the gel was heated to 150 °C for 3 days under rotation in a Teflon-lined autoclave. The CHA product was recovered by filtration and

washed several times with water, followed by calcination at 580 °C for 3 h to remove the TMAdaOH. Copper ions were introduced by suspending the calcined CHA in 250 mL (per gram zeolite) of 5 mM copper(II) acetate solution and stirred at room temperature for 24 h. Finally, the product was filtered, washed, and calcined in air at 500 °C for 3 h. The final Cu-CHA obtained and used in this work had ratios Si/Al = 15 and Cu/Al = 0.48, corresponding to a Cu content of 2.6 wt %.

The measurement of the NO conversion was done in a microreactor using a 5 mg sample of the Cu-CHA catalyst (sieve fraction 150–300 μm) in a quartz U-tube reactor with 2 mm inner diameter. The composition of the reactor exit gas was determined using a Gaset CX400 FTIR spectrometer connected to the outlet of the reactor. The catalyst was heated for 1 h at 550 °C, in an atmosphere of 500 ppm NO, 533 ppm NH<sub>3</sub>, 5% H<sub>2</sub>O, and 10% O<sub>2</sub> in N<sub>2</sub> at a flow rate of 225 N mL/min. The catalyst was then stepwise cooled down to 160 °C using the same flow and gas composition. In each step, the sample was kept at a constant temperature for 20 min. The conversion of NO was determined on the basis of the averaged concentration measured during the final 5 min in each step.

Spin-polarized DFT calculations were used to estimate the free energies of the reaction intermediates at 200 °C. The calculations were performed with the GPAW package<sup>87,88</sup> using a real space grid-based projector augmented wave method. A grid spacing of  $h = 0.2$  and a Fermi smearing of 0.1 K were found sufficient to obtain a satisfactory convergence of the relative energies. The BEEF-vdW functional<sup>89</sup> was used to account for the van der Waals interactions.<sup>90</sup> This functional has been shown to produce reliable results for the interaction of molecules with zeolites.<sup>91,92</sup> The free energy of the adsorbed species at 200 °C was calculated on the basis of calculated DFT energies at 0 K and the vibrational frequencies, using the thermochemistry package in ASE.<sup>93</sup> The free energies of the gas phase species at 200 °C were obtained from the Shomate equations. The zeolite was represented by periodic cells with hexagonal symmetry (cell parameters  $a, b = 13.886$  Å;  $c = 15.116$  Å;  $\alpha = 120^\circ$ ;  $\beta, \gamma = 90^\circ$ ), containing 36 T atoms.

The in situ X-ray absorption spectroscopy (XAS) measurements at the Cu K-edge were performed at the BM23 beamline of the European Synchrotron Radiation Facility (ESRF, Grenoble, France). A self-supported pellet (~100 mg) of the Cu-CHA catalyst was placed in a Microtomo reactor cell connected to a gas manifold that allowed control of the total gas flow and gas composition of the mixtures. Initially, the Cu-CHA sample was heated to 400 °C at 5 °C/min in 50% O<sub>2</sub>/He at a flow of 100 mL/min and kept at those conditions until the near-edge features (XANES) became stable (~1 h), then the temperature was reduced to 200 °C, and the catalyst was exposed to the different reaction gas mixtures.

The XAS measurements at the Cu K-edge were carried out in transmission mode, using double-crystal Si(111) monochromator and ionization chambers for the detection of the incident and transmitted photons. A copper foil was measured simultaneously as a reference for energy alignment.<sup>81</sup> For steady-state conditions, the XAS spectra were collected in a step-scan mode, at a resolution of 0.3 eV around the edge, and a step size of  $\Delta k = 0.035$  Å<sup>−1</sup> in the EXAFS part, using a dwell time of 1–4 s per point. Typically, the data analysis was based on an average of 2 consecutive scans. To monitor changes in time upon changing gas atmosphere, a faster scan mode was used, with a step resolution of 0.3 eV around the edge and a

$\Delta k = 0.08 \text{ \AA}^{-1}$  up to  $8 \text{ \AA}^{-1}$  with a dwell time of 1 s per point; this allowed for collecting about 10 scans per hour.

$[\text{Cu}^{\text{I}}(\text{NH}_3)_2]^+$  and  $[\text{Cu}^{\text{II}}(\text{NH}_3)_4]^{2+}$  complexes were used as references for the XAS measurements. Both complexes were prepared as aqueous solutions. The  $[\text{Cu}^{\text{II}}(\text{NH}_3)_4]^{2+}$  solution ( $\sim 50 \text{ mM}$ , deep violet-blue color) was prepared by dissolving tetraamminecopper(II) sulfate monohydrate (Sigma-Aldrich, 98%) in water; a small amount of  $\text{NH}_3$  was added to avoid precipitation of  $\text{Cu}(\text{OH})_2$ . The solution was poured into a glass capillary ( $\varnothing = 3.5 \text{ mm}$ ), which was used for the XAS measurement. The  $[\text{Cu}^{\text{I}}(\text{NH}_3)_2]^+$  complex was prepared by dropwise adding a solution of hydrazine (Sigma-Aldrich, 35%) into the capillary with the  $[\text{Cu}^{\text{II}}(\text{NH}_3)_4]^{2+}$  complex.<sup>94</sup> To prevent the reoxidation of  $\text{Cu}^+$  ions by  $\text{O}_2$ , the capillary was then sealed with paraffin. The  $[\text{Cu}^{\text{I}}(\text{NH}_3)_2]^+$  solution was prepared immediately before the XAS measurements.

For the FTIR measurements,  $\sim 15 \text{ mg}$  of the Cu-CHA catalyst was pressed into a self-supported pellet and placed inside a commercial FTIR reactor cell (AABSPEC, no. 2000-A multimode), which allows recording of infrared spectra under controlled temperature and gas atmosphere. Prior to the measurements, the catalyst was heated at  $400 \text{ }^\circ\text{C}$  for 30 min (heating rate  $5 \text{ }^\circ\text{C}/\text{min}$ ) in a 50%  $\text{O}_2/\text{He}$  gas mixture at a flow of  $50 \text{ mL}/\text{min}$ , then the sample was cooled to  $200 \text{ }^\circ\text{C}$  and exposed to the different reaction gas mixtures at a flow of  $50 \text{ mL}/\text{min}$ . The FTIR spectra were recorded in transmission mode with a resolution of  $2 \text{ cm}^{-1}$  on a PerkinElmer System 2000 infrared spectrophotometer equipped with a MCT detector at liquid nitrogen temperature.

The in situ EPR measurements were performed on a continuous wave X-band Bruker EMX EPR spectrometer with the ER 4102ST cavity with a Gunn diode microwave source in the field interval 220–400 mT. A quartz tube (4 mm i.d.) with a 10–20 mg sample of the Cu-CHA catalyst (150–300  $\mu\text{m}$  sieve fraction) was used, and quartz wool was used to keep the sample in place. The sample was heated using preheated atmospheric air with a Bruker EMX VT unit. The quartz tube was connected to a gas manifold, allowing for changing of the gas atmosphere in the tube within seconds. The reactant gas flow was kept at 200 N mL/min, using Brooks mass flow controllers. A Thermo Electron Corporation model 17C ammonia analyzer was used to measure the  $\text{NO}_2$  concentration in the exit gas. The EPR spectra were measured continuously during the experiment with fast sweeps ( $\sim 10 \text{ s}$ ) between 220 and 400 mT with a microwave power of 6.3 mW, a modulation frequency of 100 kHz, a modulation amplitude of 8 G, at a frequency of 9.46 GHz, and 1024 data points. The time between two spectra was  $\sim 15 \text{ s}$ .

## AUTHOR INFORMATION

### Corresponding Authors

\*E-mail: silvia.bordiga@unito.it.

\*E-mail: slmo@kemi.dtu.dk.

\*E-mail: pabb@topsoe.dk.

### Notes

The authors declare no competing financial interest.

## ACKNOWLEDGMENTS

C.L. and K.A.L. are grateful for support from the Mega-grant of the Russian Federation Government to support scientific research at Southern Federal University, No. 14.Y26.31.0001. E.B. acknowledges financial support from the Italian “

Consorzio Interuniversitario Nazionale per la Scienza e Tecnologia dei Materiali” (INSTM). S.M. acknowledges financial support by the Danish Independent Research Council DFF1335-00175 and DFF09-070250, and Carlsbergfondet for supporting the upgrade of the EPR instrument at the Department of Chemistry, DTU. Sachem is acknowledged for making TMAdaOH available.

## REFERENCES

- (1) Moliner, M.; Franch, C.; Palomares, E.; Grill, M.; Corma, A. *Chem. Commun.* **2012**, *48*, 8264–8266.
- (2) Rahkamaa-Tolonen, K.; Maunula, T.; Lomma, M.; Huuhtanen, M.; Keiski, R. L. *Catal. Today* **2005**, *100*, 217–222.
- (3) Eng, J.; Bartholomew, C. H. *J. Catal.* **1997**, *171*, 27–44.
- (4) Kato, A.; Matsuda, S.; Kamo, T.; Nakajima, F.; Kuroda, H.; Narita, T. *J. Phys. Chem.* **1981**, *119*, 4099–4102.
- (5) Topsøe, N.-Y. *Science* **1994**, *265*, 1217–1219.
- (6) Grünert, W. In *Urea-SCR Technology for DeNOx After Treatment of Diesel Exhausts*; Nova, I., Tronconi, E., Eds.; Springer Science + Business Media: New York, 2014; pp 181–219.
- (7) Wark, M.; Brückner, A.; Liese, T.; Grünert, W. *J. Catal.* **1998**, *61*, 48–61.
- (8) Went, G. T.; Leu, L.-J.; Rosin, R. R.; Bell, A. T. *J. Catal.* **1992**, *134*, 492–505.
- (9) Iwasaki, M. In *Urea-SCR Technology for DeNOx After Treatment of Diesel Exhausts*; Nova, I., Tronconi, E., Eds.; Springer: New York, 2014; pp 221–246.
- (10) Doronkin, D. E.; Casapu, M.; Günter, T.; Müller, O.; Frahm, R.; Grunwaldt, J.-D. *J. Phys. Chem. C* **2014**, *118*, 10204–10212.
- (11) Zecchina, A.; Rivallan, M.; Berlier, G.; Lamberti, C.; Ricchiardi, G. *Phys. Chem. Chem. Phys.* **2007**, *9*, 3483–3499.
- (12) Bates, S. A.; Verma, A. A.; Paolucci, C.; Parekh, A. A.; Anggara, T.; Yezzerets, A.; Schneider, W. F.; Miller, J. T.; Delgass, W. N.; Ribeiro, F. H. *J. Catal.* **2014**, *312*, 87–97.
- (13) Vennestrom, P. N. R.; Janssens, T. V. W.; Kustov, A.; Grill, M.; Puig-Molina, A.; Lundegaard, L. F.; Tiruvalam, R. R.; Concepción, P.; Corma, A. *J. Catal.* **2014**, *309*, 477–490.
- (14) Deka, U.; Juhin, A.; Eilertsen, E. A.; Emerich, H.; Green, M. A.; Korhonen, S. T.; Weckhuysen, B. M.; Beale, A. M. *J. Phys. Chem. C* **2012**, *116*, 4809–4818.
- (15) Brandenberger, S.; Kröcher, O.; Tissler, A.; Althoff, R. *Catal. Rev.* **2008**, *50*, 492–531.
- (16) Qi, G.; Wang, L.; Yang, R. T. In *Urea-SCR Technology for DeNOx After Treatment of Diesel Exhausts*; Nova, I., Tronconi, E., Eds.; Springer Science + Business Media: New York, 2014; pp 149–177.
- (17) Ruggeri, M. P.; Grossale, A.; Nova, I.; Tronconi, E.; Jirglova, H.; Sobalik, Z. *Catal. Today* **2012**, *184*, 107–114.
- (18) Berlier, G.; Zecchina, A.; Spoto, G.; Ricchiardi, G.; Bordiga, S.; Lamberti, C. *J. Catal.* **2003**, *215*, 264–270.
- (19) Čapek, L.; Dědeček, J.; Sazama, P.; Wichterlová, B. *J. Catal.* **2010**, *272*, 44–54.
- (20) Sobalik, Z.; Sazama, P.; Dedecek, J.; Wichterlová, B. *Appl. Catal., A* **2014**, *474*, 178–185.
- (21) Sazama, P.; Wichterlová, B.; Tábor, E.; Štastný, P.; Sathu, N. K.; Sobalik, Z.; Dědeček, J.; Sklenák, Š.; Klein, P.; Vondrová, A. *J. Catal.* **2014**, *312*, 123–138.
- (22) Bates, S. A.; Delgass, W. N.; Ribeiro, F. H.; Miller, J. T.; Gounder, R. *J. Catal.* **2014**, *312*, 26–36.
- (23) Schwidder, M.; Santhosh Kumar, M.; Bentrup, U.; Pérez-Ramírez, J.; Brückner, A.; Grünert, W. *Microporous Mesoporous Mater.* **2008**, *111*, 124–133.
- (24) Brandenberger, S.; Kröcher, O.; Wokaun, A.; Tissler, A.; Althoff, R. *J. Catal.* **2009**, *268*, 297–306.
- (25) Llabrés i Xamena, F. X.; Fiscaro, P.; Berlier, G.; Zecchina, A.; Turnes Palomino, G.; Prestipino, C.; Bordiga, S.; Giamello, E.; Lamberti, C. *J. Phys. Chem. B* **2003**, *107*, 7036–7044.

- (26) Turnes Palomino, G.; Fiscaro, P.; Bordiga, S.; Zecchina, A.; Giuria, V.; Giamello, E.; Lamberti, C. *J. Phys. Chem. B* **2000**, *104*, 4064–4073.
- (27) Giordanino, F.; Vennestrøm, P. N. R.; Lundegaard, L. F.; Stappen, F. N.; Mossin, S.; Beato, P.; Bordiga, S.; Lamberti, C. *Dalton Trans.* **2013**, *42*, 12741–12761.
- (28) Borfecchia, E.; Lomachenko, K. A.; Giordanino, F.; Falsig, H.; Beato, P.; Soldatov, A. V.; Bordiga, S.; Lamberti, C. *Chem. Sci.* **2015**, *6*, 548–563.
- (29) Godiksen, A.; Stappen, F. N.; Vennestrøm, P. N. R.; Giordanino, F.; Rasmussen, S. B.; Lundegaard, L. F.; Mossin, S. J. *Phys. Chem. C* **2014**, *118*, 23126–23138.
- (30) Ganemi, B.; Björnbo, E.; Paul, J. *Appl. Catal., B* **1998**, *17*, 293–311.
- (31) Woertink, J. S.; Smeets, P. J.; Groothaert, M. H.; Vance, M. A.; Sels, B. F.; Schoonheydt, R. A.; Solomon, E. I. *Proc. Natl. Acad. Sci. U.S.A.* **2009**, *106*, 18908–18913.
- (32) Smeets, P. J.; Hadt, R. G.; Woertink, J. S.; Vanelderden, P.; Schoonheydt, R. A.; Sels, B. F.; Solomon, E. I. *J. Am. Chem. Soc.* **2010**, *132*, 14736–14738.
- (33) Wang, L.; Gaudet, J. R.; Li, W.; Weng, D. *J. Catal.* **2013**, *306*, 68–77.
- (34) Deka, U.; Lezcano-Gonzalez, I.; Weckhuysen, B. M.; Beale, A. M. *ACS Catal.* **2013**, *3*, 414–427.
- (35) Wang, L.; Gaudet, J. R.; Li, W.; Weng, D. *J. Catal.* **2013**, *306*, 68–77.
- (36) Verma, A. A.; Bates, S. A.; Anggara, T.; Paolucci, C.; Parekh, A. A.; Kamasamudram, K.; Yezerets, A.; Miller, J. T.; Delgass, W. N.; Schneider, W. F.; Ribeiro, F. H. *J. Catal.* **2014**, *312*, 179–190.
- (37) Wang, D.; Zhang, L.; Li, J.; Kamasamudram, K.; Epling, W. S. *Catal. Today* **2014**, *231*, 64–74.
- (38) Tsai, M.-L.; Hadt, R. G.; Vanelderden, P.; Sels, B. F.; Schoonheydt, R. A.; Solomon, E. I. *J. Am. Chem. Soc.* **2014**, *136*, 3522–3529.
- (39) Gao, F.; Walter, E. D.; Kollar, M.; Wang, Y.; Szanyi, J.; Peden, C. H. *J. Catal.* **2014**, *319*, 1–14.
- (40) Gao, F.; Kwak, J. H.; Szanyi, J.; Peden, C. H. F. *Top. Catal.* **2013**, *56*, 1441–1459.
- (41) Andersen, C. W.; Bremholm, M.; Vennestrøm, P. N. R.; Blichfeld, A. B.; Lundegaard, L. F.; Iversen, B. B. *IUCrJ.* **2014**, *1*, 382–386.
- (42) Uzunova, E. L.; Mikosch, H.; St. Nikolov, G. *Int. J. Quantum Chem.* **2013**, *113*, 723–728.
- (43) Szanyi, J.; Kwak, J. H.; Zhu, H.; Peden, C. H. F. *Phys. Chem. Chem. Phys.* **2013**, *15*, 2368–2380.
- (44) Giordanino, F.; Borfecchia, E.; Lomachenko, K. A.; Lazzarini, A.; Agostini, G.; Gallo, E.; Soldatov, A. V.; Beato, P.; Bordiga, S.; Lamberti, C. *J. Phys. Chem. Lett.* **2014**, *5*, 1552–1559.
- (45) Göttl, F.; Hafner, J. *J. Chem. Phys.* **2012**, *136*, 064501.
- (46) Deka, U.; Lezcano-Gonzalez, I.; Warrender, S. J.; Picone, A. L.; Wright, P. A.; Weckhuysen, B. M.; Beale, A. M. *Microporous Mesoporous Mater.* **2013**, *166*, 144–152.
- (47) Xue, J.; Wang, X.; Qi, G.; Wang, J.; Shen, M.; Li, W. *J. Catal.* **2013**, *297*, 56–64.
- (48) Göttl, F.; Buló, R. E.; Hafner, J.; Sautet, P. *J. Phys. Chem. Lett.* **2013**, *4*, 2244–2249.
- (49) Kieger, S.; Delahay, G.; Coq, B.; Neveu, B. *J. Catal.* **1999**, *183*, 267–280.
- (50) Yu, T.; Hao, T.; Fan, D.; Wang, J.; Shen, M.; Li, W. *J. Phys. Chem. C* **2014**, *118*, 6565–6575.
- (51) Paolucci, C.; Verma, A. A.; Bates, S. A.; Kispersky, V. F.; Miller, J. T.; Gounder, R.; Delgass, W. N.; Ribeiro, F. H.; Schneider, W. F. *Angew. Chem., Int. Ed.* **2014**, *53*, 11828–11833.
- (52) McEwen, J. S.; Anggara, T.; Schneider, W. F.; Kispersky, V. F.; Miller, J. T.; Delgass, W. N.; Ribeiro, F. H. *Catal. Today* **2012**, *184*, 129–144.
- (53) Kispersky, V. F.; Kropf, A. J.; Ribeiro, F. H.; Miller, J. T. *Phys. Chem. Chem. Phys.* **2012**, *14*, 2229–2238.
- (54) Prestipino, C.; Berlier, G.; Llabrés i Xamena, F.; Spoto, G.; Bordiga, S.; Zecchina, A.; Turnes Palomino, G.; Yamamoto, T.; Lamberti, C. *Chem. Phys. Lett.* **2002**, *363*, 389–396.
- (55) Colombo, M.; Nova, I.; Tronconi, E. *Catal. Today* **2010**, *151*, 223–230.
- (56) Long, R.; Yang, R. *J. Catal.* **2002**, *207*, 274–285.
- (57) Wallin, M. *J. Catal.* **2003**, *218*, 354–364.
- (58) Devadas, M.; Kröcher, O.; Elsener, M.; Wokaun, A.; Mitrikas, G.; Söger, N.; Pfeifer, M.; Demel, Y.; Mussmann, L. *Catal. Today* **2007**, *119*, 137–144.
- (59) Metkar, P. S.; Balakotaiah, V.; Harold, M. P. *Catal. Today* **2012**, *184*, 115–128.
- (60) Ciardelli, C.; Nova, I.; Tronconi, E.; Bandl-Konrad, B. *Chem. Commun.* **2004**, 2718–2719.
- (61) Grossale, A.; Nova, I.; Tronconi, E.; Chatterjee, D.; Weibel, M. *J. Catal.* **2008**, *256*, 312–322.
- (62) Colombo, M.; Nova, I.; Tronconi, E. *Catal. Today* **2012**, *197*, 243–255.
- (63) Wang, D.; Zhang, L.; Kamasamudram, K.; Epling, W. *ACS Catal.* **2013**, *3*, 871–881.
- (64) Tronconi, E.; Nova, I. In *Urea-SCR Technology for deNO<sub>x</sub> After Treatment of Diesel Exhausts*. Nova, I., Tronconi, E., Eds.; Springer Science + Business Media: New York, 2014; pp 247–270.
- (65) Mihai, O.; Widyastuti, C. R.; Ando, S.; Kamasamudram, K.; Li, J.; Joshi, S. Y.; Currier, N. W.; Yezerets, A.; Olsson, L. *J. Catal.* **2014**, *311*, 170–181.
- (66) Ruggeri, M. P.; Nova, I.; Tronconi, E. *Top. Catal.* **2013**, *56*, 109–113.
- (67) Delahay, G.; Valade, D.; Guzmán-Vargas, A.; Coq, B. *Appl. Catal., B* **2005**, *55*, 149–155.
- (68) Lamberti, C.; Groppo, E.; Spoto, G.; Bordiga, S.; Zecchina, A. *Adv. Catal.* **2007**, *51*, 1–74.
- (69) Poignant, F.; Freysz, J. L.; Daturi, M.; Saussey, J. *Catal. Today* **2001**, *70*, 197–211.
- (70) Sedlmair, C.; Gil, B.; Seshan, K.; Jentys, A.; Lercher, J. A. *Phys. Chem. Chem. Phys.* **2003**, *5*, 1897–1905.
- (71) Colombo, M.; Nova, I.; Tronconi, E. *Appl. Catal., B* **2012**, *111*–*112*, 433–444.
- (72) Gao, F.; Walter, E. D.; Karp, E. M.; Luo, J.; Tonkyn, R. G.; Kwak, J. H.; Szanyi, J.; Peden, C. H. F. *J. Catal.* **2013**, *300*, 20–29.
- (73) Korhonen, S. T.; Fickel, D. W.; Lobo, R. F.; Weckhuysen, B. M.; Beale, A. M. *Chem. Commun.* **2011**, *47*, 800–802.
- (74) Zhang, R.; McEwen, J.-S.; Kollár, M.; Gao, F.; Wang, Y.; Szanyi, J.; Peden, C. H. F. *ACS Catal.* **2014**, *4*, 4093–4105.
- (75) Hadjiivanov, K. I. *Catal. Rev.* **2000**, *42*, 71–144.
- (76) Lamble, G.; Moen, A.; Nicholson, D. G. *J. Chem. Soc. Faraday Trans.* **1994**, *90*, 2211–2213.
- (77) Kau, L. S.; Spira-Solomon, D. J.; Penner-Hahn, J. E.; Hodgson, K. O.; Solomon, E. I. *J. Am. Chem. Soc.* **1987**, *109*, 6433–6442.
- (78) Sano, M.; Komorita, S.; Yamatera, H. *Inorg. Chem.* **1992**, *31*, 459–463.
- (79) Lamberti, C.; Spoto, G.; Scarano, D.; Pazé, C.; Salvalaggio, M.; Bordiga, S.; Zecchina, A.; Turnes Palomino, G.; D’Acapito, F. *Chem. Phys. Lett.* **1997**, *269*, 500–508.
- (80) Groothaert, M. H.; van Bokhoven, J. A.; Battiston, A. A.; Weckhuysen, B. M.; Schoonheydt, R. A. *J. Am. Chem. Soc.* **2003**, *125*, 7629–7640.
- (81) Bordiga, S.; Groppo, E.; Agostini, G.; van Bokhoven, J. A.; Lamberti, C. *Chem. Rev.* **2013**, *113*, 1736–850.
- (82) Kucherov, A. V.; Gerlock, J. L.; Jen, H.-W.; Shelef, M. *Zeolites* **1995**, *15*, 15–20.
- (83) Lezcano-Gonzalez, I.; Deka, U.; van der Bij, H. E.; Paalanen, P.; Arstad, B.; Weckhuysen, B. M.; Beale, A. M. *Appl. Catal., B* **2014**, *154*, 339–349.
- (84) DFT calculations of gaseous NO and NO<sub>2</sub> are known to be inaccurate, and hence, the estimate of  $\Delta G^0$  is based on the known values for  $\Delta G_f^0$  for alkali nitrates and nitrites.<sup>85</sup>
- (85) *CRC Handbook of Chemistry and Physics*, 78 th ed.; Lide, D. R., Ed.; CRC Press: Boca Raton, FL, 1997.

- (86) Tsukahara, H.; Ishida, T.; Mayumi, M. *Nitric Oxide* **1999**, *3*, 191–198.
- (87) Mortensen, J. J.; Hansen, L. B.; Jacobsen, K. W. *Phys. Rev. B* **2005**, *71*, 035109.
- (88) Enkovaara, J.; Rostgaard, C.; Mortensen, J. J.; Chen, J.; Dulak, M.; Ferrighi, L.; Gavnholt, J.; Glinsvad, C.; Haikola, V.; Hansen, H. A.; Kristoffersen, H. H.; Kuisma, M.; Larsen, A. H.; Lehtovaara, L.; Ljungberg, M.; Lopez-Acevedo, O.; Moses, P. G.; Ojanen, J.; Olsen, T.; Petzold, V.; Romero, N. A.; Stausholm-Møller, J.; Strange, M.; Tritsarlis, G. A.; Vanin, M.; Walter, M.; Hammer, B.; Häkkinen, H.; Madsen, G. K. H.; Nieminen, R. M.; Nørskov, J. K.; Puska, M.; Rantala, T. T.; Schiøtz, J.; Thygesen, K. S.; Jacobsen, K. W. *J. Phys.: Condens. Matter* **2010**, *22*, 253202.
- (89) Wellendorff, J.; Lundgaard, K. T.; Møgelhøj, A.; Petzold, V.; Landis, D. D.; Nørskov, J. K.; Bligaard, T.; Jacobsen, K. W. *Phys. Rev. B* **2012**, *85*, 235149.
- (90) Because Van der Waals interactions are expected to contribute to the binding of molecules in zeolite pores, the BEEF–vdW functional was chosen. From a comparison with similar calculations using the standard RPBE functional, we find that introduction of the Van der Waals interactions results in a change in binding energy of 0.3 eV at most for the fragments studied here.
- (91) Brogaard, R. Y.; Moses, P. G.; Nørskov, J. K. *Catal. Lett.* **2012**, *142*, 1057–1060.
- (92) Brogaard, R. Y.; Weckhuysen, B. M.; Nørskov, J. K. *J. Catal.* **2013**, *300*, 235–241.
- (93) ASE thermochemistry package. <https://wiki.fysik.dtu.dk/ase/ase/thermochemistry/thermochemistry.html>
- (94) Moen, A.; Nicholson, D. G.; Rønning, M. *J. Chem. Soc. Faraday Trans.* **1995**, *91*, 3189–3194.